Northwest Atlantic Fisheries Organization

Serial No. N6960 **NAFO SCR Doc. 19/039**

SCIENTIFIC COUNCIL MEETING – JUNE 2019

Environmental Conditions in the Labrador Sea during 2018

Igor Yashayaev, Marc Ringuette, Ingrid Peterson, Zeliang Wang, Erica Head, Stephen Punshon, Emmanuel Devred, Kumiko Azetsu-Scott

Department of Fisheries and Oceans, Maritimes Region
Ocean and Ecosystem Sciences Division, Bedford Institute of Oceanography
P.O. Box 1006, Dartmouth, N.S. B2Y 4A2

Abstract

In the Labrador Sea, wintertime surface heat losses result in the formation of dense waters which plays an important role in ventilating the deep ocean and driving the global ocean overturning circulation. In the winter of 2017-18, as in the previous two winters, the mid-high latitude North Atlantic experienced more moderate surface heat loss in the region than in the winter of 2014-15, characterized by the highest heat losses in more than two decades. The winter (Dec-Mar) NAO index in 2017-18 and winter heat fluxes in the central Labrador Sea were near-normal. However, a high atmospheric pressure anomaly extended throughout the Labrador Sea in winter, resulting in above-normal air and sea surface temperatures in the western Labrador Sea, and below-normal temperatures in the northeastern Labrador Sea. For SST, these conditions persisted into the spring, but appeared to have propagated cyclonically. Sea ice concentration anomalies in February and March 2018 were generally negative in the western Labrador Sea, and positive in the northeastern Labrador Sea, consistent with atmospheric circulation and air temperatures. Ocean temperature in the central Labrador Sea was near-normal, and continued a negative trend observed since 2010 for the 15-100 m layer, and since 2011 for the 200-2000 m layer caused by deepening of winter convection. Despite a reduction in the cumulative heat losses from the sea surface after 2014-15, the depth of winter convection continued to increase resulting in the most significant formation, in terms of volume, density and depth, of Labrador Sea Water (LSW) since 1994 reaching below 2000 m. This is mainly due to the water column preconditioning caused by convective mixing in the previous years. Bedford Institute of Oceanography North Atlantic model simulations suggest however that the transport of the Labrador Current decreased between 1995 and 2014, but has since increased slightly.

Both total carbon and SF6 averaged over the top 1000 m showed an increasing trend in the past decade, reflecting continuation of uptake of the anthropogenic gases by the subpolar North Atlantic. This trend was accompanied by a reduction in pH level critical for marine ecosystems. However, the CFC-12 concentration is presently significantly lower than in the previous decade which is likely related to the reduction in the CFC emissions observed since the start of the century.

Extensive cloud covers form April to June of 2018 reduced the percent coverage of the Labrador Shelf/Slope and Central Basin regions with ocean colour data to less than 20% in any of the seven days composite, and most of the good pixels were provided by the northeast corner of the box. Missing an important portion of the bloom initiation phase made it difficult to estimate its extent and magnitude. Although the general tendencies go toward lower abundances in general for copepods, the three largest *Calanus* species abundances are larger than average in the Labrador basin.

Introduction

The extreme losses of the oceanic heat to the atmosphere occurring in the Labrador Sea in winter of most years result in the formation of relatively dense water masses spreading through and consequently ventilating the intermediate and deep layers in the North Atlantic Ocean. Recurrent production of dense waters also makes the Labrador Sea a principal co-driver of the global ocean overturning circulation.

Temperature, salinity, density, dissolved oxygen and other environmental variables characterizing the upper layer of the Labrador Sea respond to many factors, including atmospheric forcing, runoff, precipitation, warm and saline inflows from the adjacent North Atlantic basins and colder fresher water arriving from Arctic and glacier melt. Consequently, the variability in the physical, chemical and biological properties of the upper layer of the Labrador Sea is strongly affected by seasonal, interannual and decadal variability in the affecting factors.

A moderately to anomalously cold winter cooling of the upper layer can result in increase in the surface density cause the water column to mix to great depths. By the end of winter, convective mixing (hence the name of the process – winter convection) may penetrate deeper than 1500 m and in extreme cases deeper than 2000 m. Convection is known to ventilate the deeper ocean with atmospheric gases while pumping the nutrients abundant in the deeper layers back to the surface. Reduced surface heat losses in milder winters lead to weaker convection, and as a result to stronger influence of heat and salt passed from the warm and saline Atlantic Waters. As a result a stronger stratification gets established in the subsurface (>200 m) and deeper layers during the period of convective relaxation. Year-specific atmospheric conditions, partly expressed in cumulative heat flux and other climate indices, and their year-to-year persistence play a dominant role in setting the deep convection events in the Labrador Sea, which can help explain development of significant long-term oceanographic phenomena in the region. One of the most commonly used climate indices is the North Atlantic Oscillation (NAO) index. It expressed the strength of zonal atmospheric circulation in the North Atlantic. An increase in the zonal wind is often paired with strengthening of the atmospheric forcing leading to surface higher heat losses in winter. Under the global warming scenarios, the increasing freshwater inputs from Greenland glacier melting and the Arctic also contribute to the oceanographic variations at seasonal, inter-annual and longer time scales. However, the recent study suggests (Dukhovskoy et al., 2019) that the effect of Greenland freshwater flux anomaly brought by the observed acceleration of Greenland Ice Sheet (GIS) melt is not sufficient to fully explain the present changes in water column salinity and convective activity. However, the future may bring a different example, especially if the GIS melt continues to accelerate.

While the changes below 2500 m, except for the bottom layer about 200 m thick, are rather monotonic, there have been significant decade-long recurrent warm and cold events in the upper 2000 m. A period of warming and increasing salinity during the mid-1960s to mid-1970s was followed by an inverse period of cooling and freshening during the 1990s. This period was characterized by deep winter convection that filled the upper 2.0 to 2.5 kilometers of the Labrador Sea with cold, dense and relatively fresh water. Milder winters in the early 2000s produced more limited amounts of mode waters, which have gradually become warmer, saltier, and less dense than in the previous decade. The cessation of extreme convection in the mid-1990s led to the upward temperature and downward density trends spanning the upper 1000 m of the water column that were interrupted in the winters of 1999-2000, 2001-02, 2007-08 and 2011-12, and finally reversed in 2013-14, when deep convection was observed reaching and exceeding the depth of 1500 m over significant parts of the central Labrador Sea. In the four most recent consecutive winters, 2013-14, 2014-15, 2015-16 and 2017-18 and 2017-18, deep convection kept getting deeper and deeper with each new event, while the convectively formed water mass, so-called Labrador Sea Water (LSW), was getting colder and denser as convection deepened. The environmental conditions that contributed to the case of deep convection in 2007-08 have been documented by Yashayaev and Loder (2009). The most recent intensification of winter convection, 2011-12 through 2015-16, has been analyzed by Yashayaev and Loder (2016 and 2017). Finally, the most recent episodes of deepening convection, 2016-17 and 2017-18, are presented in the last year and present reports.

About one quarter of carbon dioxide (CO_2) released by human activities (anthropogenic CO_2, mainly due to fossil fuel combustion) has been taken up by the oceans, altering the basic ocean chemistry, specifically the marine carbonate system. The Labrador Sea is the site of a strong "solubility pump"; anthropogenic CO_2 sequestrated from the atmosphere is transported to the deep ocean by chemical and physical processes. On the flip side however, the dissolution of anthropogenic CO_2 also has decreased ocean pH by 0.1 units over the past 200 years, corresponding to a 30% increase in acidity (Caldeira and Wickett, 2003). If global emissions of

CO_2 continue at their present rate, ocean pH is predicted to fall an additional 0.3 units by 2100. The oceans have not experienced such a rapid pH decrease (ocean acidification) or one of this great a magnitude for at least 20 million years (Feely et al., 2004), raising serious concerns about the ability of marine ecosystems to adapt. The major impact of decreasing pH will be felt by organisms that form calcium carbonate ($CaCO_3$) shells and skeletons, because rising acidity increases the solubility of $CaCO_3$. Since $CaCO_3$ shells and skeletons are naturally more soluble at lower temperatures and higher pressures, high latitude and deep water ecosystems will be more vulnerable to the added stress of ocean acidification. Furthermore, rapid environmental changes such as retreating ice extent and enhanced hydrological cycles may amplify these problems.

Light limits primary production and phytoplankton communities succession for much of the year (Harrison and Li, 2008; Fragoso et al, 2016) and shallow mixed layer and Nitrate is limiting phytoplankton growth on the Labrador Shelf while Silicate seems to be the limiting factor for growth in the Labrador Basin (Harrison and Li 2008). These conditions favour the emergence of *Phaeocystis pouchetii* in the North and Eastern part of the Labrador Sea (Fragoso et al 2016). The Labrador Shelf, mostly under the influence of Arctic water masses, is dominated by polar diatom species (*Thalassiosira* spp. and *Bacteriosira bathyomphala*) and species associated with costal melting ice (*Porosira glacialis* and *Fossula arctica)*. Primary production patterns and mesoscale features leave their imprint on the mesozooplankton distribution and abundances (Yebra et al 2009). One species of copepod, *Calanus finmarchicus*, dominates the mesozooplankton biomass throughout the central region of the Labrador Sea, while on the shelves two Arctic *Calanus* species, *C. glacialis* and *C. hyperboreus*, are equally important. *C. finmarchicus* abundances show regional variations that are generally consistent from year-to-year and are related to differences in the timing of the life-cycle events, which are themselves influenced by environmental conditions. In spring, populations have generally few young stages from the new years' generations. Total abundance in spring showed an upward but insignificant trend on the Labrador Shelf between 1996 and 2012. In the Central Labrador Sea total *C. finmarchicus* abundance is generally relatively low in spring and summer, with a low proportion of young stages; one exception being the summer of 1995, when young stages were dominant and total abundance was relatively high. There was no trend in springtime total abundance between 1996 and 2012 and the abundance in 2012 was within the range seen in previous springs. *C. finmarchicus* abundances are generally higher in the eastern Labrador Sea (the area most influenced by the Irminger Current) than farther west during spring time because the earlier spring bloom generally leadeading to earlier reproduction in *C. finmarchicus*. Although abundances are generally higher here in summer than in spring, the highest concentration of all occurred in spring 2006.

Production variability in the lower trophic compartments eventually impacts the higher trophic growth and recruitment and ultimately influences commercial fisheries in the region.

Since 1990, the Ocean and Ecosystem Sciences Division at the Bedford Institute of Oceanography (BIO) has carried out annual occupations of an oceanographic section across the Labrador Sea (Figure 1). The section was designated as AR7W (Atlantic Repeat Hydrography Line 7 West) in the World Ocean Circulation Experiment (WOCE) hydrography line classification (notation). These surveys cover a wide range of physical and chemical characteristics and properties of seawater, e.g., temperature, salinity, density, currents, dissolved oxygen, nutrients, chlorofluorocarbons, sulfur hexafluoride, total inorganic carbon, pH, oxygen and iodine isotopes, and measurements of important biological and ecosystem variables, e.g., bacteria until 2012, phytoplankton and mesozooplankton.

The AR7W oceanographic line is presently regarded as the major component of the Atlantic Zone Off-shelf Monitoring Program (AZOMP) of Fisheries and Oceans Canada (DFO) and its annual occupation is recognized as the most vital and significant Canadian contribution to the international Global Climate Observing System (GCOS) and to the (international) Climate Variability (CLIVAR) component of the World Climate Research Programme (WCRP). It is also reported on annually as a part of the environmental synopsis submitted by DFO to the Northwest Atlantic Fisheries organisation (NAFO) for the fish stock assessment within the region. The AR7W section spans approximately 900 km from Misery Point, Labrador, to Cape Desolation, Greenland, however the shelf areas can be out of reach and hence limited in data coverage due to sea-ice condition. With nearly three decades of annual surveys, the time series now allows a examination of multiyear trends in all key ecosystem variables. DFO also contributes to the international Argo program by deploying floats in the Labrador Sea and managing, processing and analysing the Argo data. The annual AZOMP multidisciplinary survey of the Labrador Sea, primarily consisting of AR7W occupations, mooring redeployments and Argo float deployments, represent an invaluable contribution to the ongoing international ocean and climate monitoring

and research effort and is highlight in a recent special issue of Progress in Oceanography (Yashayaev et al., 2015; Kieke and Yashayaev, 2015) and the latest publications in Nature (Thornalley et al., 2018) and Science (Lozier et al., 2019).

In addition to the AR7W Line, a full AZOMP survey also includes sampling of the extended Halifax Line (XHL) to monitor variability on the Scotian Rise and Slope in the deep western boundary flows of the North Atlantic and to obtain additional information on oceanographic properties and lower-trophic-level variability of the Slope Water affecting the Scotian and adjacent shelves (http://www.bio.gc.ca/science/monitoring-monitorage/azomp-pmzao/azomp-pmzao-en.php).

In May of 2018, the Atlantic Repeat 7-West (AR7W) line was occupied by the BIO for the 31st time since 1990. The shipboard observations collected in the 2018 AZOMP mission carried on the CCGS Hudson, Commanding Officer Captain F.B.H. Francey (Figure 1) as well as from the past cruises, Argo float profiles to 2000 m and remote-sensed measurement are used for monitoring of year-round variability of the oceanographic conditions in the Labrador Sea presented here.

Data Sources and Methods of Analysis

The state of the Labrador Sea environment in 2018 as presented in this report is based on a synthesis of ship survey and profiling float data, remote-sensed measurement and reanalysis products, and ocean model simulations. The sources of these data are described in the present section.

Atmospheric Reanalysis

The NCEP/NCAR Reanalysis Project is a joint project between the National Centers for Environmental Prediction (NCEP) and the National Center for Atmospheric Research (NCAR), often referred to as the NCAR/NCEP reanalysis. The goal of this joint effort is to produce new Surface Air Temperature and Sea Surface analysis using historical data (1948 onwards) to produce analyses of the current atmospheric state (Kalnay et al., 1996).

North Atlantic Oscillation Index

The North Atlantic Oscillation (NAO) index used here is the difference in winter (December, January and February) sea level atmospheric pressures between the Azores and Iceland, and is a measure of the strength of the winter westerly winds over the Northwest Atlantic and represents the dominant, large scale meteorological forcing over the North Atlantic Ocean. Specifically, the index was calculated using observed monthly sea level pressures at Ponta Delgada (up to 1997, 2009-2015), Santa Maria (1998-2005), and Lajes (2006-2008) in the Azores, and at Akureyri in Iceland. A small number of missing data early in the time series were filled using pressures from nearby stations.

Ice cover

The sea ice concentrations from satellite passive microwave data are obtained from the U.S. National Snow and Ice Data Center (Cavalieri et al., 1996; Meier et al., 2017).

Ship Survey Data

Our primary data sources are *(i)* full-depth temperature, salinity, and dissolved oxygen profiles on the AR7W (Atlantic Repeat Hydrography Line 7 West) line across the Labrador Sea occupied during Fisheries and Oceans Canada's (DFO's) annual ship-based survey under its Atlantic Zone Off-shelf Monitoring Program (AZOMP), *(ii)* temperature and salinity profiles over the upper 2000 m in the Labrador Sea region from the International Argo float program (discussed in the following section), *(iii)* publically available observed-level temperature and salinity data archived by other programs and national and international data centers (e.g., Kieke and Yashayaev, 2015), and *(iv)* a near-bottom moored temperature time series from a long-term mooring maintained by the BIO on the Labrador Slope.

The main data additions to the previous years are observations from Argo floats up to March 2019 and DFO's annual conductivity-temperature-depth (CTD) survey of the AR7W line across the Labrador Sea in May 2018 (Figure 1).

The AZOMP survey is a continuation of annual DFO occupations of the AR7W line by BIO since the start of the World Ocean Circulation Experiment (WOCE) in 1990 (Lazier et al., 2002; Yashayaev et al., 2015). Since 2004, the survey has been carried out mostly in May with at least 30 CTD and water sampling (e.g., for dissolved oxygen, nutrients, transient tracer) stations occupied between Labrador and Greenland. The pressure, temperature, conductivity, salinity, and dissolved oxygen data sets have been quality controlled and calibrated to meet WOCE standards, using water sample (e.g., Autosal salinity and Winkler titration), SBE35 temperature recorder and laboratory calibration data. Argo float temperature and salinity profiles, available since 2002, have been quality controlled through comparisons with vessel CTD and water sample data and comparisons between floats and by performing critical analyses of spatial and temporal deviations. The historical and other recent data have also been quality controlled and processed through similar critical analyses (see Yashayaev and Seidov, 2015, for a summary).

Following Yashayaev and Loder (2009, 2016 and 2017), but now including all available Argo and ship-based survey data to March 2019, time-depth series of spatially averaged potential temperature, salinity, and potential density with weekly-to-monthly (dependent on Argo and ship survey data coverage) resolution have been computed for an area of ~60,000 km^2 in the central Labrador Sea.

Time series of parameter values at selected depths have been estimated from all individual profiles in the central Labrador Sea and then low-pass-filtered to provide annual indices of variability since 1987.

Further, to place the recent variability in a historical context, we use annual time series of temperature, salinity, and density averaged over the 15-100 and 200-2000 m vertical intervals in the central Labrador Sea back to 1938 as long-term indices of these variables over its upper and intermediate-depth waters. These were derived from time series for selected depths like those discussed above and previously reported.

Finally, in examining the influence of atmospheric forcing on temperature variability, two annual indices have been used: the winter (December to March) NAO index; and the cumulative air-sea heat flux integrated over individual-year cooling seasons, computed following the procedure described in Yashayaev and Loder (2009) using 6 hourly heat flux and daily-mean radiation data obtained from the U.S. National Centers for Environmental Prediction (NCEP) Reanalysis (R2).

Profiling Argo Float Data

Argo is an international network of profiling floats collecting high-quality temperature and salinity profiles from the upper 2000 m of the ice-free global ocean and through float displacements currents from intermediate depths. For most of a typical 10-day cycle a battery-powered autonomous float freely drifts at a “parking depth” of usually 1000 m, where its position is stabilised through buoyant adjustment. Once the float is released from its parking depth it descents to approximately 2000 m and then ascents to the surface, while profiling temperature, salinity and other variables, if additional sensors are installed. When the surface is reached the acquired data get transmitted, and the float sinks back to its parking depth. Since 2002, the near real-time temperature and salinity Argo float data collectively draw a large-scale picture of the oceanographic structure and circulation of the Labrador Sea. The array is typically used to reconstruct the seasonal and interannual variability of the physical characteristics and dissolved oxygen in the upper 2000 m water column. The value of the Argo floats is signified in winter, when they work out to be the only mean to provide information about real-time development of winter convection.

Ocean Colour

Ocean colour, as an indicator of sea surface chlorophyll-*a* concentration (SSC), is derived from the observations made by the Moderate Resolution Imaging Spectroradiometer (MODIS) aboard the Aqua Earth Observing System satellite between 2003 and 2012 and by the Visible Infrared Imaging Radiometer Suite (VIIRS) since 2013. Remotely-sensed images of ocean colour for the Labrador Sea are composited on a weekly (bi-weekly before 2013) basis from the beginning of March to the end of October each year. Between November and February, the data are usually too sparse to be useful. From these composites, ocean colour data are extracted from 511 pixels covering the AR7W transect. A weekly climatology of SSC constructed from the time series of ocean colour since 2013 (bi-weekly from 2003 to 2013), and fitted with a Gaussian function to extract the principals blooms metrics following Zhai et al (2011). If a satellite composite has less than 20% in spatial data

coverage it becomes difficult to compute meaningful blooms indices, particularly between May and June It then became a case-by-case decision.

Phytoplankton

Standard method protocols were used to record hydrographic profiles, to collect water samples, and to analyse nutrients and chlorophyll a as described in Mitchell et al. (2002). Two replicates of 100 ml aliquots are drawn from at 100, 80, 60, 50, 40, 30, 20, 10 m and sea surface and filtered via vacuum filtration onto 25 mm glass fibre filters (GFF). After the filtration the glass fiber filters are deposited into separate scintillation vials containing 10 ml of 90% acetone and stored at -20°C for 24 hour to allow the extraction of the chlorophyll-*a* pigments. Algal pigments, particularly chlorophyll-*a*, fluoresce in the red wavelengths after extraction in acetone when they are excited by blue wavelengths of light. The fluorometer excites the extracted sample with a broadband blue light and the resulting fluorescence in the red is detected by a photomultiplier (Holm-Hansen et al. 1965). The significant fluorescence by phaeopigments is corrected for by acidifying the sample which converts all of the chlorophyll-*a* to phaeopigments. By applying a measured conversion for the relative strength of chlorophyll and phaeopigment fluorescence, the two values can be used to calculate both the chlorophyll-*a* and phaeopigment concentrations (Welschmeyer 1994).

Mesozooplankton

Mesozooplankton were collected in vertical net hauls in the upper 100 m using a 0.75 m diameter ring net fitted with a 200 μm mesh. The cod-end was attached via a clamp to a weighted hydro-wire and the towing bridle was attached to a crossbow mounted on the wire at a height above the cod-end such that the net was held vertically. In this configuration zooplankton were only collected as the net was towed upwards. The towing speed was ca 0.5 m s^{-1} and the volume of water sampled was assumed to be the volume of the cylinder sampled by the net until 2010, when filtered volume were then measured using Danemark K/C flowmeter equipped with a back-spin pin preventing the impeller to spin on the descent of the net, only measuring flow on the ascent of the net. Samples were preserved in 2% formalin. For *C. finmarchicus*, *C. hyperboreus* and *C. glacialis*, size frequency distributions of sizes-at-stage were constructed for all stages at each station and distinguished between developmental stages. Other taxa were identified to the level of species (sometimes to stage), genus or group, depending on their abundance in the samples. 300 organisms and a minimum of 200 *Calanus spp* is required in order to obtain a meaningful abundance respectively for the community structure and the *Calanus* population growth.

The phytoplankton and mesozooplankton data were complemented with CTD temperature values averaged between the sea surface and 100 m (dbar) at the CTD cast locations corresponding to biological sampling. The uppermost measurement from each down trace CTD profile with one metre (dbar) resolution was extrapolated to the sea surface to achieve consistency of vertical averaging between the profiles.

Continuous Plankton Recorder Data

The Continuous Plankton Recorder (CPR) is an instrument that is towed by commercial ships that collects plankton at a depth of ~7 m on a long continuous ribbon of silk (~260 μm mesh). The position on the silk corresponds to the location of the different sampling stations. CPR data are analysed to detect changes in indices of phytoplankton concentration (colour and relative numerical abundance) and zooplankton relative abundance for different months, years and/or decades in the northwest Atlantic. The indices indicate relative changes in concentration (Richardson et al. 2006). The sampling methods from the first surveys in the northwest Atlantic (1957 for the sub-polar gyre, 1960 for the Canadian continental shelf) to the present are exactly the same so that valid comparisons can be made between months, years and decades. CPR data collected from January to December 2014 were only made available in January 2016 to add to the DFO data archive.

The tow routes between Reykjavik and the Gulf of Maine are divided into eight regions: the Western Scotian Shelf (WSS), the Eastern Scotian Shelf (ESS), the South Newfoundland Shelf (SNS), the Newfoundland Shelf (NS) and four regions in the NW Atlantic sub-polar gyre, divided into 5 degree of longitude bins (Figure 15). In this report a broad-scale comparison is presented for CPR data collected in all regions and all sampling decades. More detailed analyses for the Scotian Shelf and Newfoundland Shelf regions are presented in the annual AZMP Reports from the Maritimes and Newfoundland Regions. These latter reports concentrate on data collected since 1992, since these are comparable to AZMP survey results, which date back to 1999.

Monthly average abundances (log_{10}(N+1) transformed for all but PCI) were calculated for 15 CPR taxa by averaging values for all individual samples collected within each region for each month and year. These regional monthly average abundances were then averaged by month for samples collected within each decade prior to 2009, (i.e. 1960-1969, 1970-1979, 1980-1989, 1990-1999 and 2000-2009) to give decadal monthly average abundances, which were then averaged for each decade to give decadal annual average abundances. During the 1980s sampling was too infrequent to calculate decadal annual average abundances, except for the three regions between 30 and 45oW, and even in these regions there was no sampling in January or December. The averages of the monthly values for the 1970s and 1990s were used to fill in these missing months, however, so that decadal annual average abundances could be calculated. The averages of the decadal annual average abundances over the 4 or 5 sampling decades represent the climatological average annual abundances. Four-year annual average abundances were calculated for 2010-2013, using the 4-year monthly averages, and annual average abundances were calculated for 2014, where possible. According to the protocol used here, annual averages for individual years can only be calculated if there was sampling in more than 8 months, with no gaps of more than 2 consecutive months (linear interpolation being used to fill in for missing months). These criteria were met in 7 regions in 2014, for which there were 0-3 missing months, with no 2 or 3 month gaps. No annual average abundances could be calculated for the SNS region in 2014, since there was sampling in only 6 months and a 5 month gap.

Standardized abundance anomalies were calculated for the decadal (1960s, 1970s, 1980s, 1990s, 2000s), four-year (2010-2013) and annual (2014) average abundances, by subtracting the climatological average annual abundances for each time period, and by dividing the differences by the standard deviations calculated for the annual average abundances available for the individual years between 1992 and 2009. Sampling coverage was good everywhere over this period, so that annual averages could be calculated for 13-15 individual years in all regions. The underlying assumption of this approach to the calculation of the standardized abundance anomalies is that inter-annual variability was similar for all decades. This assumption was found to be reasonable for the 1960-1970s in the four regions of the sub-polar gyre, decades for which annual average abundances and standard deviations could be calculated for 15 individual years. As well, it was not inconsistent with results for the shelf regions, where annual averages over the same decades could be calculated for only 2-6 years.

Results and Discussion

North Atlantic Oscillation (NAO) Index

The NAO is an important teleconnection pattern influencing atmospheric processes in the Labrador Sea (Barnston and Livezey, 1987; Hausser et al., 2015). The NAO index is based on the surface sea-level pressure difference between the Subtropical (Azores) High and the Subpolar (Icelandic) Low. The positive phase of the NAO reflects below-normal heights and pressure across the high latitudes of the North Atlantic and above-normal heights and pressure over the central North Atlantic, the eastern United States and western Europe. The negative phase reflects an opposite pattern of height and pressure anomalies over these regions. Both NAO phases are associated with basin-wide changes in the intensity and location of the North Atlantic jet stream and storm track, and in large-scale modulations of the zonal and meridional heat and moisture transport (Hurrell, 1995), resulting in the modification of the temperature and precipitation patterns.

The NAO exhibits considerable interseasonal to interdecadal variability, and prolonged periods of both positive and negative phases seem to have more influence on convection in the Labrador Sea than short-term fluctuations (Yashayaev, 2007). Yashayaev and Loder (2017) further showed that the ocean's memory or inter-annual preconditioning plays and important role in switching between the regimes of deeper and shallower convection. Even though this was demonstrated on the cumulative winter heat losses (updated below), a similar connection exists between lag-filtered NAO, convection depth and ocean heat content. The wintertime NAO also exhibits significant multi-decadal variability (Hurrell, 1995). An upward trend of the NAO index from the 1960s through the 1990s was noted by Visbeck et al (2001), although since the peak in the 1990s there has been a slight downward trend. Recent studies reveal an atmospheric circulation pattern, complementary to NAO, which becomes more prominent in years of low NAO (Hausser et al., 2015). Further study of this phenomenon will help to improve understanding and forecasting capabilities of atmospheric and oceanic conditions.

NAO index anomalies (relative to the 1981-2010 mean) computed using two versions of the NAO index are shown in Figure 2 (upper panel). The station-based NAO index (green) is the difference in winter (December, January, February, March) sea level atmospheric pressure between the Azores and Iceland (Hurrell et al., 2018), and is a measure of the strength of the winter westerly winds over the Northwest Atlantic. The PC-based NAO index (blue) is associated with the first empirical orthogonal function (EOF) of standardized monthly 500-mb height anomaly fields for the Northern Hemisphere. The spatial pattern of this EOF shows a high over southern Greenland, and a low near the latitude of the Azores.

In 2010, the NAO index reached a record low (Figure 2, upper panel), with surface heat losses being quite low as well, leading to warmer than normal oceanic conditions as we show in both the Argo float and AR7W survey based records. In 2011, the NAO index rebounded from the record low but still remained well below the 30-year average (1981-2010). In 2012, however, the NAO index was strongly positive, up to a level comparable to those in early 1990s showing the highest winter index over the last twenty years. There was a significant change in the winter NAO index in 2013, when it became moderately negative. In 2014, the NAO index returned to its high positive phase, slightly lower than the 2012 value, making it the second highest in the last twenty years, leading to colder than normal winter conditions in the region. In 2015 there was another high NAO event, as a matter of fact, it was the highest value on record – the largest positive NAO magnitude in the 122 year record. In 2017, the winter NAO index was slightly positive in both versions, but significantly smaller than in 2012, 2015 and even 2016 (Figure 2, upper panel).

In 2018, the station-based NAO anomaly (green) was slightly negative, while the PC-based NAO anomaly (blue) was weakly positive. In both cases, the NAO has decreased from the extremely high values observed in 2015.

The lower panel of Figure 2 shows a map of sea level pressure (SLP) anomalies in winter 2018 (December, January, February, March) over the North Atlantic relative to the 1981-2010 mean. A large high pressure anomaly can be seen extending from Davis Strait southward past the Azores. This would be associated with stronger-than-normal southerly winds on the western side of the Labrador Sea, and northerly winds on the eastern side. A second high pressure anomaly in the Norwegian Sea would be associated with southerly winds off northeast Greenland. As one might expect, there is a high correlation between the reported changes in the NAO index and changes in the surface heat flux integrated for each cooling season (Figure 3). The cumulative winter heat losses are in turn correlated with the convection depth and heat content.

Surface Air Temperature and Sea Surface Temperature

Seasonal maps of surface air temperature anomalies from the NCEP Reanalysis are shown in Figure 3. In the winter map, a high anomaly can be seen on the western side of the Labrador Sea, and a low anomaly on the eastern side, consistent with the SLP anomalies. A high anomaly can also be seen off northeastern Greenland.

Seasonal maps of sea surface temperature anomalies (Figure 4) from the NOAA 1/4° Optimum Interpolation Sea Surface Temperature (OISST) analysis show similar patterns to the air temperature anomalies. The OISST analysis is constructed by combining observations from satellites, ships, and buoys on a regular global grid, and interpolating to fill in gaps. In the winter map, warm anomalies can be seen over most of the Labrador Sea and off northeastern Greenland, and a cold anomaly off southwestern Greenland. In spring and summer, the cold anomaly appears to propagate westward across the northern Labrador Sea, and the warm anomaly off northeastern Greenland appears to propagate around the southern tip of Greenland into the Labrador Sea. Annual maps of surface air temperature and sea surface temperature anomalies are shown in Figure 5.

Seasonal time series of seasonal air temperature anomalies for 1948-2018 at (1) Nuuk, Greenland (2) Iqaluit, Nunavut, and (3) Cartwright, Labrador are shown in Figure 6, and the annual time series are shown in Figure 7. In winter, the temperature was slightly negative for Nuuk, but slightly positive for Iqaluit and Cartwright, in agreement with the air temperature maps. In spring, air temperature anomalies are positive in all three locations, and the annual mean air temperature is near-normal at all three locations for 2018.

Monthly air temperature anomalies at the three locations are shown in Figure. 8. A strong negative air temperature anomaly can be seen in February at Nuuk, and a strong positive anomaly in March in Iqaluit and Cartwright.

Sea Ice Concentration and Extent

Monthly maps of sea ice concentration and extent, using data from the US National Snow and Ice Data Center, are shown in Figure 9. Off western Greenland in February and March, positive ice concentration anomalies can be seen, and the ice extent is higher than normal, in agreement with winter air temperature and sea surface temperature anomalies. In the western Labrador Sea, sea ice concentration is generally below normal, and ice extent is generally near-normal or below-normal.

In order to provide a quantitative and clearer view of the ice extent changes in the Davis Strait (63-68°N), the northern Labrador Sea (58-63°N), and the Labrador Shelf (53-58°N), the ice extents for the three regions were estimated by summing the areas with ice concentration higher than 85%.

Seasonal time series of sea ice extent anomalies are shown in Figure 10 for three latitude bands: (1) Davis Strait (63-68°N), (2) the Northern Labrador Sea (58-63°N), and (3) Labrador Shelf (53-58°N, and the annual time series are shown in Figure 11. For winter, spring, and the annual means, ice extent anomalies in 2018 are positive for Davis Strait, but negative for the Northern Labrador Sea, and Labrador Shelf.

Mean monthly sea ice extent from December 2017 to June 2018 for the three regions is shown in Figure 12, along with mean monthly ice extent for 1981-2010. For Davis Strait, ice extent is below-normal in December to January, but is above-normal from February to June. For the Northern Labrador Sea, ice extent is below-normal from December to April, but near-normal from May to June. For the Labrador Shelf, ice extent is below-normal from December to June.

Winter Convection and Hydrographic Conditions in the Central Labrador Sea

The advent of the International Argo Program has provided the oceanographic community with unprecedented, year-round observations of temperature and salinity in the Labrador Sea. The Argo dataset is our only source of *in-situ* data available for year-round monitoring of oceanographic conditions in the Labrador Sea. Time-depth distributions of seawater temperature and salinity based on all Argo and ship survey profile data available in the central Labrador Sea for the time period of 2002-2019 in the depth range of 0-2000 m are presented in Figure 14. The time series clearly demonstrates the seasonal and inter-annual variability over the last decade and a half in this region. The deep convection event of 2008 is evident in both the temperature and salinity fields. The conditions in the winter of 2011 were similar to those in the preceding winter with very limited convection (mixed layer depths did not exceed 800 m). Then, in the winter of 2012, convection reached the depths of ~1400 m, which is clearly present in temperature and salinity profiles acquired by both Argo floats and ship survey. Salinity in the top 200 m in 2012 was the lowest since 2003, particularly in the top 50 m. Convection also occurred in the winter of 2013, but it was not as deep as in the previous year, and was mostly limited to the top 1000 m. The situation changed quite significantly in 2014. Wintertime cooling triggered convective mixing homogenizing the top 1600 m and probably even deeper layer in the central Labrador Sea. Over the following four winters convection developed to nearly 2000 m making this whole part of the water column colder and denser with each cooling cycle. This pattern agrees with previously stated impact of a multiyear recurrence of relatively strong cooling coming in phase with high NAO and resulting in preconditioning of water column which in turn facilitates development of an even deeper convection in a following year even if the strength of winter cooling has declined.

The annual mean water column properties (temperature, salinity and density) averaged over the top 2000 m, NAO index, and cumulated surface heat losses and heat content changes in winter are presented in Figure 15. The effect of water column preconditioning by winter convection of previous years is well reflected in the one-side low-pass filtered curves indicated in the figure over the line connecting cumulative winter heat losses and the NAO bar graph.

Other than being the main factor of interannual variability of the intermediate layer throughout the North Atlantic, wintertime convection in the Labrador Sea is a key process driving or strongly influencing the Atlantic Meridional Overturning Circulation (AMOC), and the Labrador Sea steps here as one of the few areas in the global ocean where the surface waters are exchanged with those from much greater depths. This process also has an important role in biogeochemical cycling in the Labrador Sea, and strong convection enhances the entrainment of gases such as oxygen and carbon dioxide into the deep water from the atmosphere, as well as from upper-layer freshwater.

In the winter of 2017-18, as in the previous two winters, the mid-high latitude North Atlantic experienced a more moderate heat loss to the atmosphere than in the winter of 2014 15 (which had the highest surface heat loss in more than two decades). The cumulative surface heat losses in the Labrador Sea were also the lowest since the winter of 2013-14. Despite of the reduction in winter heat losses, the depth of winter convection has been steadily increasing since 2014-15, forming, as a result, the most significant, in terms of volume, depth and density, class of Labrador Sea Water (LSW) since 1994. Such persistency in LSW development seen as the deep cold water cascading in the time evolution of vertical temperature and salinity profiles (Figure 14) owes to the water column preconditioning sustained at the intermediate depths over the previous years. The temperature and salinity profiles obtained by the Argo floats show that the winter mixed layer and hence convection in the central Labrador Sea reached and even exceeded 2000 m in 2018, continuing the tendency of winter mixed layer deepening going on for seven years (Figure 14). This suggests that certain properties, such as low temperature, weak vertical stability and weak overall stratification, imposed on the water column by the stronger-than-usual convective mixing in the previous years, had resulted in a kind of preconditioning that facilitated further development of deep convection this year (Figure 15). A reservoir filled with this newly ventilated, record deep, cold and fairly fresh LSW is evident in seawater property sections (Figure 16). The 2018 vintage of LSW is associated with low temperature (< 3.3°C) and salinity (< 34.86) between 1000 and 2000 m. The winter convection in the recent time period, 2015-2018, especially in the winter of 2017-18, is arguably the deepest since the record-deep cooling that reached 2400 m in 1994. The present LSW year class is one of the largest ever observed outside of the early 1990s.

The progressive cooling of the top 2000 m, and deep and intense winter mixing during the five consecutive winters of 2013-14 through 2017-18 have interrupted the general warming and stratification-building trend that has persisted in the intermediate waters of the Labrador Sea since the mid-1990s.

Interannual variability in Labrador Sea ocean heat content and cumulative surface heat loss during the cooling seasons indicates that anomalously strong winter atmospheric cooling associated with the North Atlantic Oscillation is continuing to drive the recurrent convection. In turn, recurrent deep convection is contributing to decadal-scale variability in deep-water properties and transport across and from the subpolar North Atlantic (by the ocean's western boundary and interior pathways) and potentially in the Atlantic Meridional Overturning Circulation.

Both upper, 15-100 m, and deeper, 200-2000 m, layers have been cooling since 2010 (Figure 15). However, the freshening trend seen in the newly-formed or newly-ventilated LSW between 2011 and 2016, reversed in 2016, making the LSW formed in the winter of 2017-18 the densest since the mid-1990s.

The strong winter convection in the winter of 2017-18 further added to increased gas (dissolved oxygen, anthropogenic gases, and carbon dioxide) uptakes and consequently increased gas concentrations in the Labrador Sea in the lower part of the 0-2000 m layer.

Variations of the Labrador Current

The variations of the Labrador Current (LC) can be seen as an indicator for the changes in the subpolar North Atlantic circulation, which region plays an important role in the global climate due to the winter convection event in the Labrador Sea. The variations of the LC are often connected to the variations of the AMOC. Here we present the variations of barotropic transports of the LC from an eddy resolving model developed at Bedford Institute of Oceanography (BNAM, Brickman et al. [2015], Wang et al. [2016], Brickman et al. [2018] and Wang et al. [2018]).

The BNAM model used in this study is based on NEMO 2.3 (Nucleus for European Modelling of the Ocean). It includes an ocean component OPA and a sea ice module LIM (Louvain-la-Neuve Sea Ice Model). The model domain was selected to include the North Atlantic Ocean (7°N – 75°N and 100°W – 25°E) with a nominal resolution of 1/12°. The model has a maximum of 50 levels in the vertical, with level thickness increasing from 1 m at the surface to 200 m at a depth of 1250 m and reaching the maximum value of 460 m at the bottom of the deep basins. The maximum depth represented in the model is 5730 m.

Open boundary data are from the GLORYS reanalysis product (Global Ocean ReanalYses and Simulations). The model surface forcing is taken from from a combination of CORE (Coordinated Ocean-ice Reference Experiments) and NCEP/NCAR reanalysis forcing. Model forcing variables include air temperature, wind

velocities and humidity; daily short- and long-wave radiation, and total precipitation (rain plus snow). No surface restoring to sea surface temperature is applied. However, the model's sea surface salinity is restored to its monthly climatology with a 60-day restoring time scale.

The model was spun-up for 10 years using the CORE normal year forcing. The 10-year spin-up simulation is initialized with a January climatology of temperature and salinity (T-S). The T-S climatology combines the Polar Science Center Hydrographic Climatology (PHC2.1) at high latitudes with the T-S climatology of WOA5 at middle and low latitudes.

An EOF analysis of the model output by Wang et al. [2016] (Figure 17) suggests that the variability in the Labrador Current can be partitioned into a western Labrador Current (WLC; from the 300-2500 m isobaths), and an eastern Labrador Current (ELC; from the 2500-3300 m isobaths). Following the definition of the WLC and ELC, we calculated the transports of ELC and WLC, and also those of LC (the summation of the ECL and WLC). Note: the transports are calculated based on modelled flows through the western segment of the AR7W transect.

Figure 18 shows the transport anomalies for the LC, ELC and WLC. It demonstrates that the WLC in 2018 was marginally stronger than that in 2017, about 2 Sv above the mean from 1990 to 2018, as it had been since 2001.

The declining trend of the ELC was continuing since 1996, which year had a significant drop in the winter NAO index. Wang et al. [2016] suggested the ELC is an indicator for the changes in the AMOC, which suggests that the declining trend of AMOC was continuing from this model simulation. Quantitatively speaking, the ELC in 2018 showed sign of gaining strength, it was ~4 Sv stronger that that in 2017, though it was still ~2 Sv below the 1990-2018 average The stronger ELC in 2018 suggests a possible significant strengthening of the AMOC since 2014 from the BNAM hindcast.

Total Inorganic Carbon and pH

Arctic outflow and the local uptake of anthropogenic CO_2 in the deep convection region of the Labrador Sea are major controlling mechanisms for the state of ocean acidification in the Northwest Atlantic. The Arctic water inflows into the highly productive regions in the Northwest Atlantic, which have important commercial fisheries, make these regions more susceptible to future ocean acidification than other regions (Azetsu-Scott et al., 2010). The Labrador Sea is the site of a strong "solubility pump"; anthropogenic CO_2 sequestration from the atmosphere is transported to the deep ocean by chemical and physical processes. In the layer convicted between 150 and 500 m of depth for stations in the central part of the Labrador Basin, DIC (Dissolved Inorganic Carbon) increased by 18.52 μmol kg^{-1} from 1996 to 2018, reaching a maximum of 2166.5 μmol kg^{-1}, due to the local uptake of anthropogenic CO_2 (Figure 19). As a result, the pH decreased by 0.07 units (in the total pH scale) during the same period (Figure 19) representing a decline rate of 0.003 y^{-1}, higher than the global average of 0.002 y^{-1}. Despite the slight differences observed in the metrics over the last few years, observed trends between 1996 to 2018 remain highly significant with R^2 explaining respectively 91% and 79% of the variance for DIC and pH. Ocean acidification influences the capacity of the ocean to take up CO_2 from the atmosphere. Continued monitoring of the chemical state and investigation of biological responses to ocean acidification in the Northwest Atlantic are urgently needed.

Transient Tracers CFC-12 and SF6

During the second half of the twentieth century, the atmospheric burden of chlorofluorocarbons (CFCs) increased steadily due mainly to their widespread use as refrigerants and aerosol propellants. The invasive atmospheric flux of these mostly inert gases provides an excellent record of ocean circulation, and profiles of dissolved CFC-12 concentration have been measured annually along the AR7W line since 1991. As a consequence of restrictions on the manufacture and use of ozone depleting substances introduced in 1989, the atmospheric mixing ratio of CFC-12 has been in decline since 2003 and so it is becoming less useful as a tracer of very recent ventilation. Measurements of an alternative transient tracer, sulphur hexafluoride (SF6), were introduced in 2011. There has been a rapid near-linear increase in atmospheric SF6 since around 1980 and dissolved concentration profiles show enhanced structure in recently ventilated water compared with CFC-12. Figure 20 shows mean concentrations of CFC-12 and SF6 in the 150-500 m depth layer in the central Labrador Sea basin from 1991 to present.

Ocean Color from Remote Sensing

Generally, the annual phytoplankton spring bloom starts earlier on the Greenland Shelf and Slope (mid-April to May), than in the central Labrador Basin and Labrador Shelf regions (early May to late June). An important exception was the spring of 2015, when the timing of the bloom was particularly early in the central basin, starting mid-April, one of the earliest onset since 2002. While brief, at only about 49 days in duration, this bloom was unusually intense with the highest amplitude ever recorded for the region (over 5 mg m^{-3}) and giving a seasonally integrated value among the highest ever seen. Greenland shelf characteristics followed the same pattern, while the Labrador Shelf bloom metrics were about average for the region within the two-dimensional spatial regional boxes defined by Harrison and Li (2008).

In 2018, high cloud coverage again from February to July led to a very poor ocean colour data coverage of the Labrador Shelf/Slope and in the Labrador Basin during the spring bloom period, as shown in the weekly composite images (Figure 21). The Labrador Shelf/Slope saw 10 weeks out of 17 with a data coverage lower than 10% and only 7 weeks have a coverage over 20 %. According to the Gaussian bloom parameter, the bloom started late at around the 140 day and last only 28 days for a magnitude of 96 slightly below average (Figure 22).

Despite continuing convection and general water column cooling the spring bloom observed in 2018 was not as lower than average in the Labrador Basin and Shelf/slope and also seems to begin much later than average. The limited data ocean colour data of 2018 did not allow us to make a broader spatial assessment of the bloom extent; however the few available pixels available suggest that the situation with the spring bloom leads to typically lower than average metric.

Surface temperature and Chlorophyll

Temperature recorded by the CTD during the occupation average between 100-0m correspond to the temperature regime experienced by the organism hereby measured. While the timing of the cruise may have an effect the averages, by removing the years 2003 and 2004, sampled later in June, from the reference period only lowered the reference average by 0.2°C and have little effect on the anomalies pattern (not shown). Having only stations in the slopes can also have an impact on the average temperature per region when looking at the time series and that is why the anomaly for the Labrador shelf/slope is largely positive, while the Central Basin and the Greenland Shelf/Slope are both below average a trend consistently observed since 2013 (Figure 23).

Measured chlorophyll-*a* during the occupation of AR7W largely agree with the Ocean color picture showing lower than average chlorophyll on the Labrador shelf/slope and the Central Basin, and an average chlorophyll-*a* abundance on the Greenland Shelf/Slope. The first half of the 2010s was mostly high in chlorophyll-*a* concentration, while the second half was mostly low. 2015 was an anomalously high year for chlorophyll-*a* (Figure 24). Upper ocean (z<100m) phytoplankton sampled on AR7W in the spring and early summer between 1994 and 2015 shows region-specific characteristics (Fragoso et al 20167; Li and Harrison 2014). The Greenland Shelf/Slope (GS/S) is a region with high concentrations of chlorophyll-*a* and nanophytoplankton, but low concentrations of picophytoplankton. Conversely, the central Labrador Basin is a region with lower concentrations of chlorophyll-*a* and nanophytoplankton, but high concentrations of picophytoplankton and bacteria. The Labrador Shelf/Slope (LS/S) has the lowest concentrations of chlorophyll-*a* and nanophytoplankton, but intermediate concentrations of picophytoplankton. During May 2018, concentrations of chlorophyll-*a* on the Labrador Shelf/Slope (LS/S) and in the Labrador Basin (LB) region start to rise at an average date. Phytoplankton community structure and finer taxonomy will be assessed using HPLC pigment analysis and flowcytometry from which results are not available yet.

Mesozooplankton

One species of copepod, *Calanus finmarchicus*, dominates the mesozooplankton biomass in the central region of the Labrador Sea, while on the shelves *C. finmarchicus*, *C. glacialis* and *C. hyperboreus* each contribute about one third (Head et al. 2003). *C. finmarchicus* abundances show regional variations that are generally consistent from year-to-year and are related to regional differences in the timing of the life-cycle events, which are themselves influenced by environmental conditions. On the Labrador Shelf, *C. finmarchicus* abundances are generally relatively low in spring (Figure 26), as was the case in 2018. There was no significant trend in springtime abundance of *C. finmarchicus* between 1996 and 2018 on the Labrador Shelf. In the Central Labrador

Sea, total *C. finmarchicus* abundance is generally relatively low in spring and summer, with a low proportion of young stages; one exception being the summer of 1995, when young stages were dominant and total abundance was relatively high. There was no trend in springtime total abundance between 1996 and 2015 in the Labrador Basin and the abundance in 2015 was near the low values seen in previous springs. *C. finmarchicus* abundances are generally higher in the eastern Labrador Sea than farther west in spring where the spring bloom starts earlier here, which leads to earlier reproduction in *C. finmarchicus*. Abundances are generally higher in summer than in spring, with the highest concentration of all occurring in spring 2006. The abundance in 2015 was at the low end of the range of values seen in previous springs, and there was no trend in springtime abundance between 1996 and 2014. *C. glacialis* show the same tendencies since 2014, while *C. hyperboreus* abundance lays more around the average, at the exception of 2018, matching the colder water masses in Labrador basin (Figure 26)

Pseudocalanidae are persistently more abundant then the average in the Labrador basin over the last 10 years whereas a general decreasing trend is observed on LS/S and GS/S since 2014 (Figure 27). *Oithonidae*, on the contrary, are persistently less abundant in the Labrador basin for more than 10 years, while the decrease on both slope/shelves as became more prevalent around 2014 (Figure 27). Since 2014 *Euphausiids* display general trends of lower abundance across the entire Labrador Sea (Figure 28). *Amphipods* show higher than average abundances in the Labrador Basin in 2018. Being a species associate with Arctic Water masses the phenomenon make sense given the tendencies of cooler water masses than usual temperatures in the Labrador Basin, one would expect the tendency to more prevalent (Figure 28).

Continuous Plankton Recorder

As a reminder, timeseries results pertaining to this section end in 2017 because handling of the samples is time consuming and data are only released with a year lag. The tow routes between Reykjavik and the Gulf of Maine are divided into eight regions: the Western Scotian Shelf (WSS), the Eastern Scotian Shelf (ESS), the South Newfoundland Shelf (SNS), the Newfoundland Shelf (NS) and four regions in the NW Atlantic sub-polar gyre (Figure 29).

Phytoplankton

Climatological annual phytoplankton colour index (PCI) values (1960-2009), represent the chlorophyll standing stock. In the sub-polar gyre decadal average annual PCI values shifted from low to high in all regions between the 1980s and 1990s and up until today. In 2017 PCI's are the highest east of Newfoundland Shelf regions and remained intermediate from there westward. (Figure 30). The same tendencies were observed for diatoms and dinoflagellates at the decadal scale prior to 2009. Even the slightly lower than average in the eastern regions for both groups was nevertheless part of the same increasing trend. A disconnect between the trends observes in chlorophyll abundance (PCI) and the diatom and dinoflagellates where the record high abundance of the former is only matched with around average for diatom and lower than average anomalies for the dinoflagellates.

Mesozooplankton

Since the 1980s climatological annual abundances for *Calanus* I-IV (mostly *Calanus finmarchicus*) and C. *finmarchicus* V-VI are similar in most regions, at the exception of the Scotian Shelf where the older stages below average (Figure 31). Climatological annual abundances for *C. glacialis* are low in most regions, with a very lowest anomaly in WWS and the highest value at 40-45 (Figure 31). Decadal abundance anomalies increased slightly in all regions over the decades to maximum values in the 1990s (NS) or 2000s (other regions). Climatological annual abundances for *C. hyperboreus* are very high in all regions in 2017. Cold water brought from Deep water convection in the Labrador and Irminger Sea might contribute to the resurgence of higher abundance of *C. hyperboreus* in the Northeastern Atlantic region. In most regions decadal abundance anomalies were close to average between the 1960s and 2000s, but in the 25-30°W region, the abundance anomaly was high in the 1970s, decreasing thereafter, with lowest values in 2010-2013 and 2014.

In 2017, the climatological abundances of the three small copepod groups (*Nauplii*, *Para/Pseudocalanus* and *Oithona*) shows positives anomalies within all regions at the exception of the Scotian Shelf (ESS and WWS) where *para/pseudocalanus* and Oithona are respectively very low or close to average (Figure 32). In the sub-polar gyre, decadal annual anomalies for *copepod nauplii* and *Paracalanus/Pseudocalanus* have been higher since the 1990s than they were in previous decades. On the shelf regions however while the decadal annual

abundance anomalies for copepod nauplii follows the same pattern, it is completely inverted for *Para/Pseudocalanus*, with relatively higher anomalies until the 1990s and low abundance ever since including in 2017. the 1970s and 1990s and remained ever since. Decadal annual abundances for *Oithona* spp. were generally close to average throughout all regions until the 2000s: thereafter they remained close to average in most regions, but were higher than average in the 40-45°W region in 2010-2013 and on the NS in 2014.

Macrozooplankton

Climatological annual abundances for euphausiids and hyperiid amphipods are mainly higher in the deep ocean regions of the sub-polar gyre and are highest in the 40-45°W region (Figure N). In the sub-polar gyre euphausiid decadal abundance anomalies were generally close to average until the 2000s, but since then have been lower than average. In shelf regions euphausiid abundance anomalies have shown a downward trend since the 1970s. Abundance anomalies for hyperiid amphipods follows an increasing trends in all regions in the 1960s. Compared with previous decades, although only for the NS region in the 2000s and the 25-30°W region values break that trend with lower values from average.

Summary

The Atlantic Zone Off-Shelf Monitoring Program (AZOMP) of Fisheries and Oceans Canada provides observations of variability in the ocean climate, ventilation and plankton affecting the regional climate and ecosystems off Atlantic Canada as well as the global climate system. In May of 2018, the Atlantic Repeat 7-West (AR7W) line was occupied by the Bedford Institute of Oceanography for the 31st time since 1990. Additionally, the network of profiling Argo floats provided temperature and salinity data to 2000 m used for monitoring of year-round variability of the oceanographic conditions in the Labrador Sea. However, the number of the floats within the Labrador Sea during 2018 was just marginally sufficient to resolve sub-monthly variability. The future also possess a challenge to us brought by a reduced access to the research fleet which may lead to an interruption in the 31-year long unique deep-ocean observational series. An interruption like this has already happened to us once. The omission of a single year – 2017 – in precise systematic observations of the ocean state has made us rely exclusively on profiling float, remote-sensed and atmospheric reanalysis data, and ocean model simulation products for that year, limiting our ability to diagnose and predict the key oceanic characteristics.

The winter (Dec-Mar) NAO index in 2018 and winter heat fluxes in the central Labrador Sea were near-normal. However, a high atmospheric pressure anomaly extended throughout the Labrador Sea in winter, resulting in above-normal air and sea surface temperatures in the western Labrador Sea, and below-normal temperatures in the northeastern Labrador Sea. For SST, these conditions persisted into the spring, but appeared to have propagated cyclonically.

Sea ice concentration anomalies in February and March 2018 were generally negative in the western Labrador Sea, and positive in the northeastern Labrador Sea.

Ocean temperature in the central Labrador Sea was near-normal, and continued a negative trend observed since 2010 for the 15-100 m layer, and since 2011 for the 200-2000 m layer caused by deepening of winter convection.

In the Labrador Sea, surface heat losses in winter result in the formation of dense waters, which spread across the ocean ventilating its deep layers and essentially driving the global ocean overturning circulation. In the winter of 2017-18, as in the previous two winters, the mid-high latitude North Atlantic experienced more moderate surface heat loss than in the winter of 2014-15 which in its time produced the highest heat losses in more than two decades. Despite the declining heat loss from the ocean to the atmosphere since 2014-15, the water column preconditioning staged by convective mixing in the previous years led nevertheless to the most significant formation, in terms of volume and depth, of Labrador Sea Water (LSW) since 1994. Similarly to 2017, the temperature and salinity profiles obtained by the ship survey and Argo floats show that the winter mixed layer and hence convection in the central Labrador Sea penetrated below 2000 m in the reporting year (2018), exceeding the mixed layer depths of 1600, 1700, 1850 and 1900 m in 2014, 2015, 2016 and 2017, respectively. The 2018 vintage of LSW is associated with low temperature (<3.3°C) and salinity (<34.86) between 1000 and 1900 m. The winter convection developed in the last four years 2015-2018 is arguably the deepest since the record of 2500 m in 1994, and the resulting LSW year class is one of the largest ever observed outside of the

early 1990s. This also suggests that the strong winter convection in the winter of 2017-18 further added to increased gas (dissolved oxygen, anthropogenic gases, and carbon dioxide) uptakes and consequently respective gas concentrations in the Labrador Sea in the lower part of the 0-2000 m layer.

Model results suggest that the transport of the Labrador Current decreased between 1995 and 2014, but has since increased slightly.

The characterisation of the phytoplankton bloom parameters using remote-sensed Ocean color suffer another difficult year with a heavy cloud cover for most of the spring period, making the starting date of the blooms rather difficult. Most biological indicators (Ocean Colour, Chlorophyll-a, Surface temperature and mesozoolpankton abundance), tend to stay lower than the normal, a common trait since the resuming of very deep winter convection in 2014. Some notable exceptions with the slightly higher abundance of *Calanus* spp. in the Labrador Basin, perhaps suggesting a convergence zone are favorable to these cold water species. The large anomalous bloom of 2015, never transfer in a large advantage for the higher trophic levels.

Acknowledgements

We thank the Commanding Officer of CCGS Hudson Captain F.B.H. (Fergus) Francey, the officers and the crew for their dedicated help and outstanding performance in every aspect of the 2018 AZOMP field mission. We also thank Roger Pettipas for providing the station-based air temperature data, and are grateful to the reviewers for his helpful comments and suggestions. The NCEP Reanalysis data were provided by the NOAA-CIRES Climate Diagnostics Center, Boulder, Colorado, USA, and the sea ice concentration data were provided by the US National Snow and Ice Data Center.

References

Brickman, D., Z. Wang, and B. Detracy (2015), Variability of Current Streams in Atlantic Canadian Waters: A Model Study. Atmosphere and Ocean. doi:10.1080/07055900.2015.1094026.

Brickman, D., Hebert, D., Wang, Z., 2018. Mechanism for the recent ocean warming events on the Scotian Shelf of eastern Canada. Cont. Shelf Res. 156, 11-22 https://doi.org/10.1016/j.csr.2018.01.001.

Cavalieri, D. J., C. L. Parkinson, P. Gloersen, and H. J. Zwally. 1996, updated yearly. *Sea Ice Concentrations from Nimbus-7 SMMR and DMSP SSM/I-SSMIS Passive Microwave Data, Version 1*. [north/monthly]. Boulder, Colorado USA. NASA National Snow and Ice Data Center Distributed Active Archive Center. doi: https://doi.org/10.5067/8GQ8LZQVL0VL. [Accessed 05/12/2018].

Fragoso, Glaucia M., Alex J. Poulton, Igor M. Yashayaev, Erica J.H. Head, Mark C. Stinchcombe, and Duncan A. Purdie. Biogeographical Patterns and Environmental Controls of Phytoplankton Communities from Contrasting Hydrographical Zones of the Labrador Sea. Progress in Oceanography 141 (February 2016): 212–26. doi:10.1016/j.pocean.2015.12.007.

Barnston, A. G., and R. E. Livezey (1987), Classification, seasonality and persistence of low-frequency atmospheric circulation patterns. Mon. Wea. Rev., 115, 1083-1126.

Caldeira, K., and M. E. Wickett (2003), Anthropogenic carbon and ocean pH, Nature, 425, 365

Climate Prediction Center (2010), NOAA/National Weather Service, National Centers for Environmental Prediction. Camp Springs, MA. http://www.cpc.noaa.gov/products/precip/CWlink/daily_ao_index/ao.shtml#publication

Egge, J., and Aksnes, D.L. (1992), Silicate as regulating nutrient in phytoplankton competition. Mar. Ecol. Prog. Ser. **83**(2-3): 281–289. doi: 10.3354/meps083281.

Fetterer, F., K. Knowles, W. Meier, and M. Savoie (2002), updated 2011. Sea ice index. Boulder, CO: National Snow and Ice Data Center. Digital media.

Feely, R. A., C. L. Sabine, K. Lee, W. Berelson, J. Kleypas, V. J. Fabry,and F. J. Millero (2004), Impact of anthropogenic CO_2 on the $CaCO_3$system in the oceans, Science, 305, 362–366.

Fragoso, G.M., Poulton, A.J., Yashayaev, I.M., Head, E.J.H., Stinchcombe, M.C., and Purdie, D.A. 2016. Biogeographical patterns and environmental controls of phytoplankton communities from contrasting hydrographical zones of the Labrador Sea. Progress in Oceanography 141: 212–226. doi:10.1016/j.pocean.2015.12.007.

Harrison, W.G. and W.K.W. Li (2008), Phytoplankton growth and regulation in the Labrador Sea: light and nutrient limitation. J. Northwest. Atl. Fish. 39:71-82.

Hauser, T., Demirov, E., Zhu, J. and I Yashayaev (2015), North Atlantic atmospheric and ocean inter-annual variability over the past fifty years – Dominant patterns and decadal shifts. Progress in Oceanography, Volume 132, March 2015, Pages 197–219.

Head, E.J.H., Harris, L.R and I Yashayaev. (2003), Distributions of *Calanus* spp. and other mesozooplankton in the Labrador Sea in relation to hydrography in spring and early summer (1995-2000). Prog. Oceanogr. 59: 1-30.

Holm-Hansen, O., Lorenzen, C.J., Holmes, R.W., and Strickland, J.D.H. 1965. Fluorometric Determination of Chlorophyll. ICES Journal of Marine Science 30(1): 3–15.

Hurrell, J. W. (1995), Decadal trends in the North Atlantic Oscillation: Regional temperatures and precipitation. Science, 269, 676-679.

Hurrell, J. W. and National Center for Atmospheric Research Staff (Eds). Last modified 04 Aug 2018. "The Climate Data Guide: Hurrell North Atlantic Oscillation (NAO) Index (station-based)." Retrieved from https://climatedataguide.ucar.edu/climate-data/hurrell-north-atlantic-oscillation-nao-index-station-based.

Josey, S., J. Grist, D. Kieke, I. Yashayaev, and L. Yu (2015), Sidebar: Extraordinary ocean cooling and new dense water formation in the North Atlantic [in "State of the Climate 2014"], Bull. Amer. Meteor. Soc.

Kalnay, E., M. Kanamitsu, R. Kistler, W. Collins, D. Deaven, L. Gandin, M. Iredell, S. Saha, G. White, J. Woollen, Y. Zhu, M. Chelliah, W. Ebisuzaki, W. Higgins, J. Janowiak, K.C. Mo, C. Ropelewski, J. Wang, A. Leetmaa, R. Reynolds, R. Jenne, and D. Joseph (1996), The NCEP/NCAR 40-Year Reanalysis Project., Bull. Amer. Meteor. Soc., 77, No. 3, 437-470.

Li, W.K.W. and W.G. Harisson, 2014, The state of phytoplankton and bacterioplankton and bacterioplankton in the Labrador Sea: Atlantic Zone Off-Shelf Monitoring Program 1994-2013. Can. Tech. Rep. Hydrogr. Ocean. Sci. 302:xviii+181p.

Meier, W. N., F. Fetterer, and A. K. Windnagel. 2017. *Near-Real-Time NOAA/NSIDC Climate Data Record of Passive Microwave Sea Ice Concentration, Version 1*. [north/daily]. doi: https://doi.org/10.7265/N5FF3QJ6. [Accessed 05/12/2018].

Mitchell, M.R., Harrison, G., Pauley, K., Gagné, A., Maillet, G., and Stain, P. 2002. Atlantic zonal monitoring program sampling protocol. Can. Tech. Rep. Hydrogr. Ocean Sci. 223: iv + 23p.

Raitsos, D.E., Lavender, S.J., Pradhan, Y., Tyrrell, T., Reid, P.C., Edwards, M. (2006), Coccolithophore bloom size variation in response to the regional environment of the subarctic North Atlantic. Limnol. Oceanogr. 51: 2122-2130.

Rey, F. (2012), Declining silicate concentrations in the Norwegian and Barents Seas. ICES J. Mar. Sci. J. Cons. **69**(2): 208–212

Richardson, A.J., Walne, John, A.W.G., Jonas, T.D., Lindley, J.A., Sims, D.W., Stevens, D. and M. Witt, (2006), Using continuous plankton recorder data. Prog. Oceanogr. 68: 27-74.

Thornalley D.J.R., D.W. Oppo, P. Ortega, J.I. Robson, C.M. Brierley, R. Davis, I.R. Hall, P. Moffa-Sanchez, N.L. Rose, P.T. Spooner, I. Yashayaev, L.D. Keigwin., (2018), Anomalously weak Labrador Sea convection and Atlantic overturning during the past 150 years. Nature, 2018; 556 (7700): 227 DOI: 10.1038/s41586-018-0007-4

Visbeck, M.H., J.W. Hurrell, L. Polvani and H.M. Cullen (2001), The North Atlantic Oscillation: Past, Present and Future. Proc. Nat. Acad. Sci., 98, 12876-12877 doi: 10.1073/pnas.231391598.

Wang, Z., D. Brickman, B. Greenan and I. Yashayaev (2016), An abrupt shift in the Labrador Current System in relation to winter NAO events. Journal of Geophysical Research: Oceans. DOI: 10.1002/2016JC011721.

Wang, Z., Lu, Y., Greenan, B., Brickman, D., and DeTracey, B., 2018. BNAM: An eddy-resolving North Atlantic Ocean model to support ocean monitoring. Can. Tech. Rep. Hydrogr. Ocean. Sci. 327: vii + 18p.

Yashayaev, I. (2007), Hydrographic changes in the Labrador Sea, 1960-2005, Progress in Oceanography, 73, 242-276.

Yashayaev, I., and J.W.Loder (2009), Enhanced production of Labrador Sea Water in 2008. Geophys. Res. Lett., 36: L01606, doi:10.1029/2008GL036162.

Yashayaev, I., and J.W.Loder (2016), Recurrent replenishment of Labrador Sea Water and associated decadal-scale variability. Journal of Geophys. Res.: Oceans, 121, 11, DOI: 10.1002/2016JC012046.

Yashayaev, I., and J.W.Loder (2017). Further intensification of deep convection in the Labrador Sea in 2016. Geophysical Research Letters, 44, 3, DOI: 10.1002/2016GL071668.

Yebra, L., Harris, R.P., Head, E.J.H., Yashayaev, I., Harris, L.R., and Hirst, A.G. (2009). Mesoscale physical variability affects zooplankton production in the Labrador Sea. Deep Sea Research Part I: Oceanographic Research Papers 56(5): 703–715.

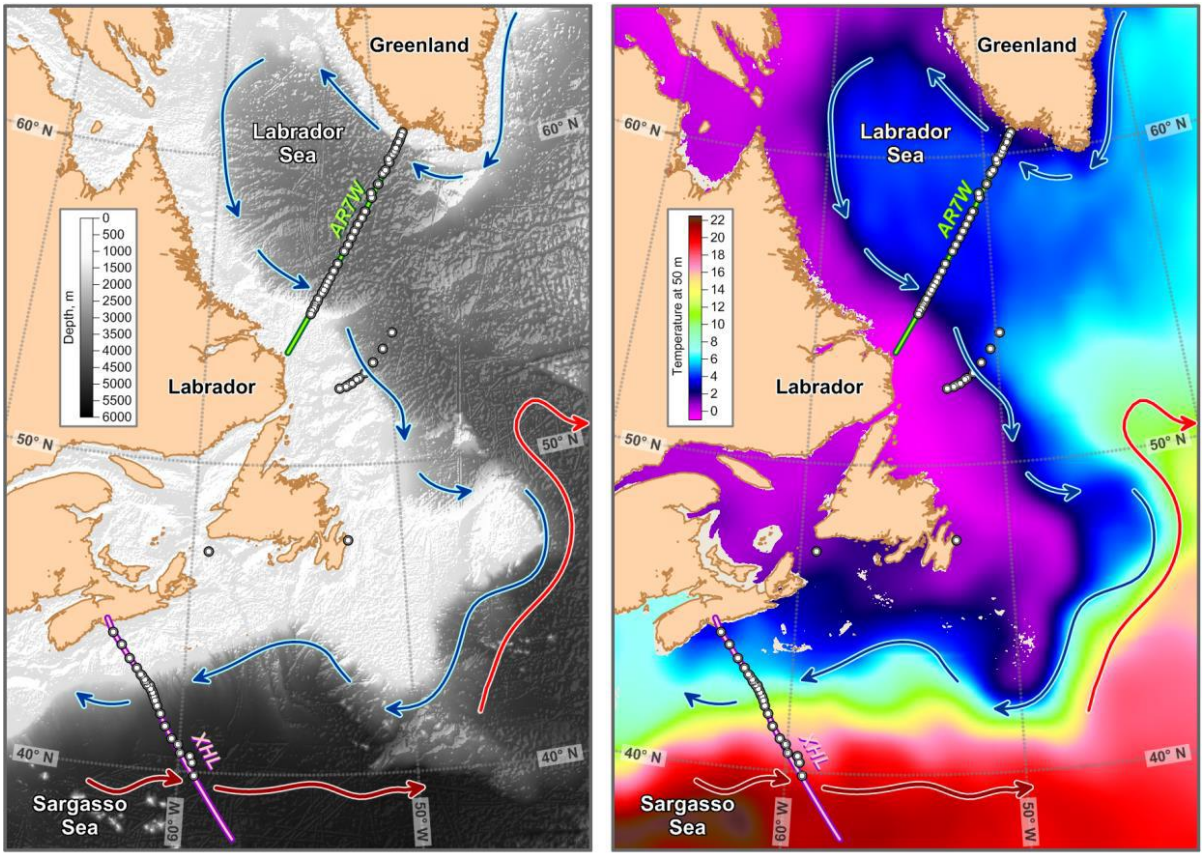

Figure 1. Topography, surface currents and temperature at 50 m in the Atlantic Zone Offshore Monitoring Program (AZOMP) domain. The CTD stations, AR7W and Extended Halifax lines occupied in the 2018 AZOMP mission, HUD2018-008, April 28 to May 24, are shown in both panels.

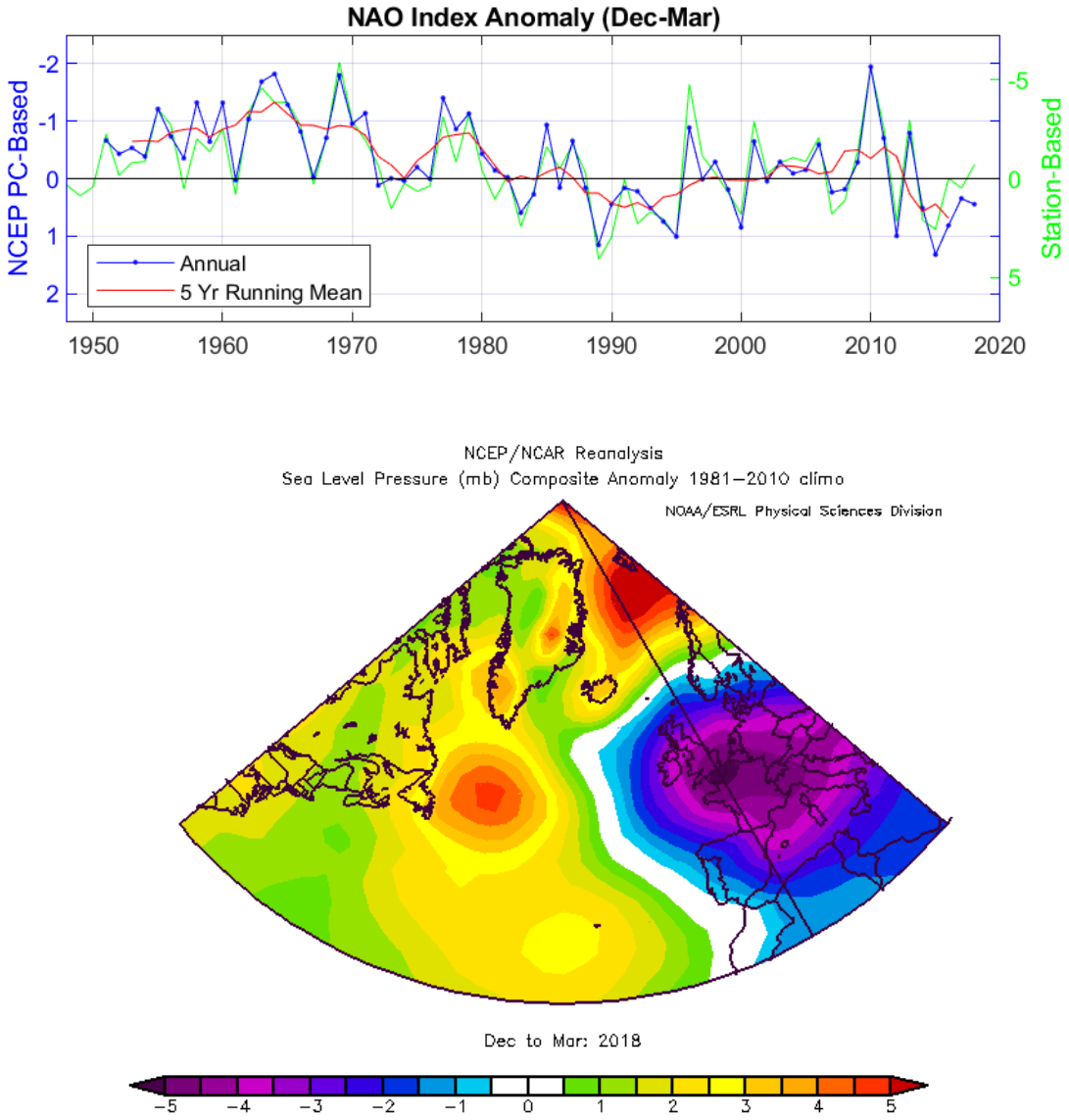

Figure 2. Anomalies of the North Atlantic Oscillation (NAO) index. The station-based NAO index (green) is defined as the winter (December, January, February, March) sea level pressure difference between the Azores and Iceland, relative to the 1981-2010 mean; data were obtained from https://climatedataguide.ucar.edu/climate-data/hurrell-north-atlantic-oscillation-nao-index-station-based (Hurrell et al. 2018). The PC-based NAO index (blue) is associated with the first empirical orthogonal function (EOF) of standardized monthly 500-mb height anomaly fields for the Northern Hemisphere; data were obtained from https://www.cpc.ncep.noaa.gov/data/teledoc/nao.shtml. The lower panel shows the 2018 December-March sea level pressure anomaly over the North Atlantic.

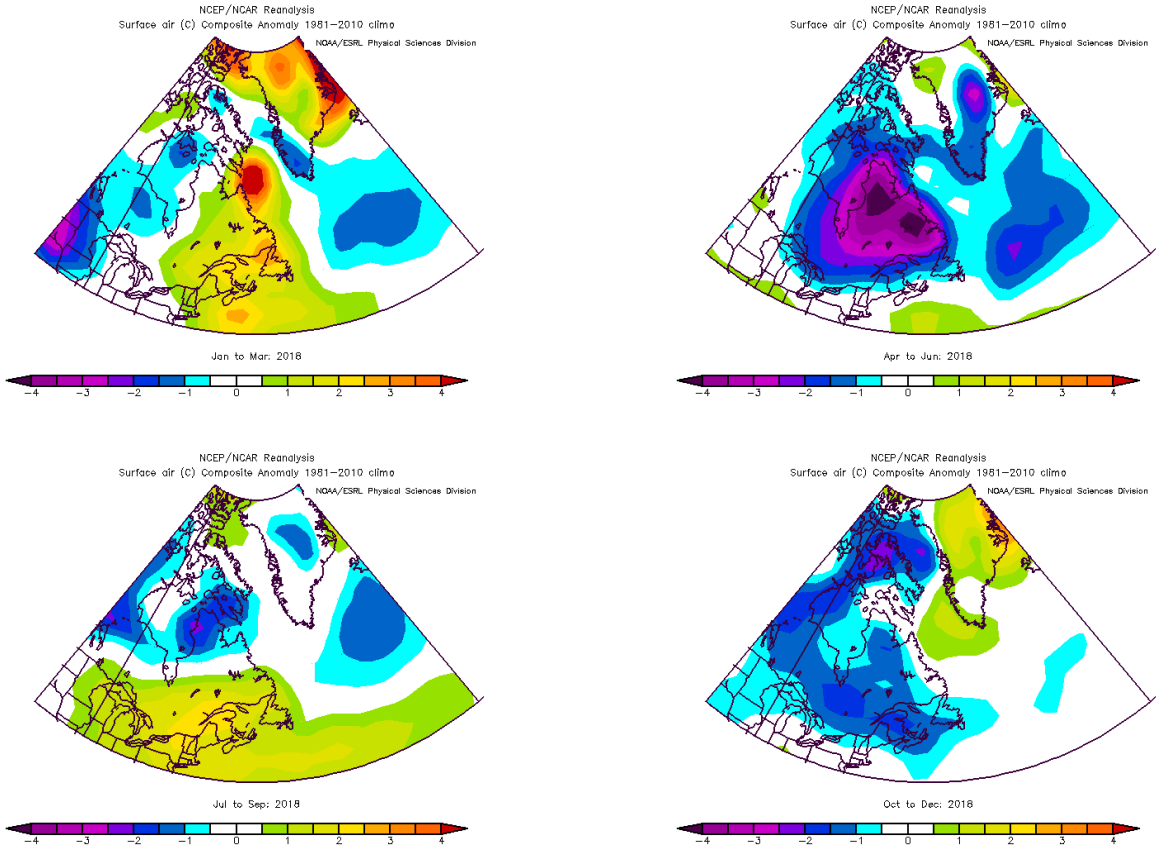

Figure 3. Seasonal air temperature anomalies (ºC) over the Northwest Atlantic relative to the 1981-2010 means; data were obtained from NOAA Internet site (accessed 30 April 2019).

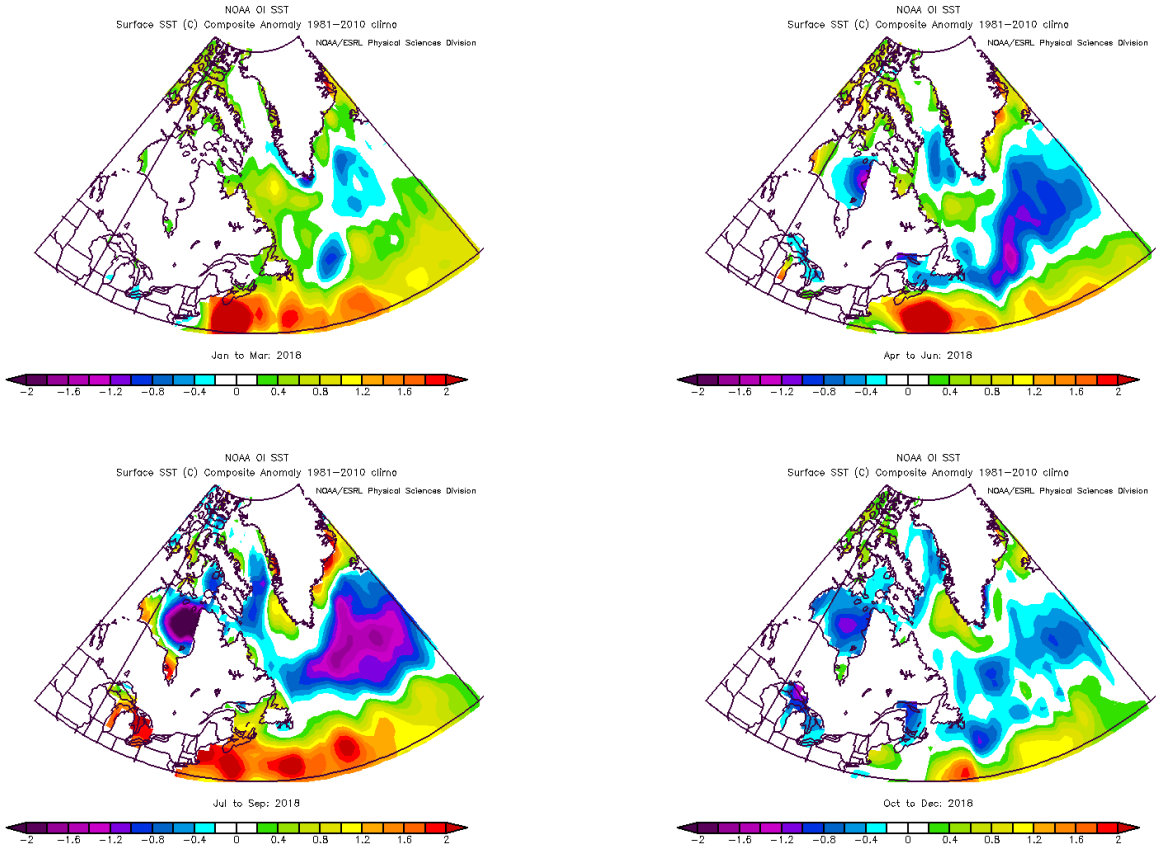

Figure 4. Seasonal sea surface temperature anomalies (ºC) over the Northwest Atlantic relative to the 1981-2010 means; data were obtained from NOAA Internet site (accessed 30 April 2019).

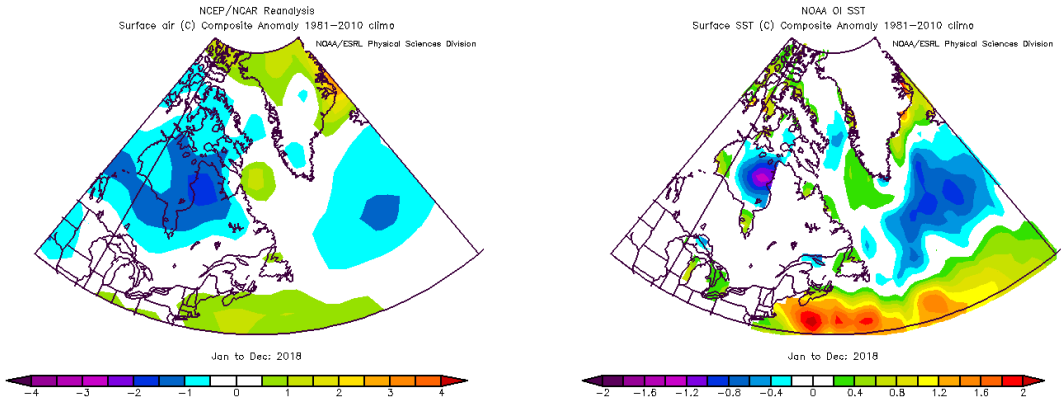

Figure 5. Annual (a) air temperature anomalies and (b) sea surface temperature anomalies (ºC) over the Northwest Atlantic relative to the 1981-2010 means; data were obtained from NOAA Internet site (accessed 30 April 2019).

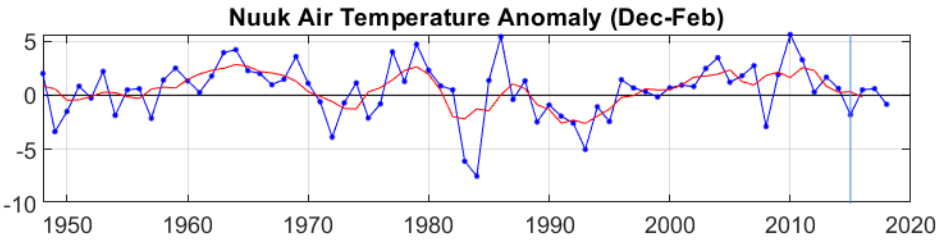
Nuuk Air Temperature Anomaly (Dec-Feb)
5
0
-5
-10
1950
1960
1970
1980
1990
2000
2010
2020

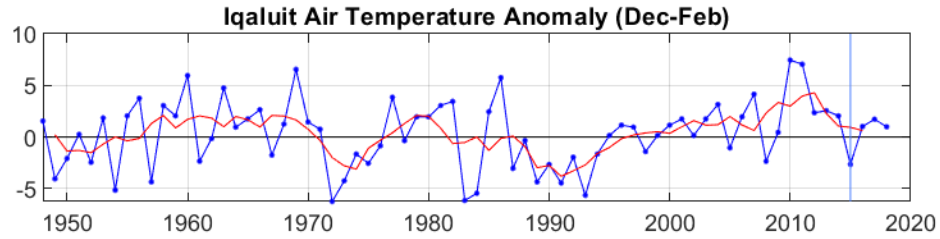
Iqaluit Air Temperature Anomaly (Dec-Feb)
10
5
0
-5
1950
1960
1970
1980
1990
2000
2010
2020

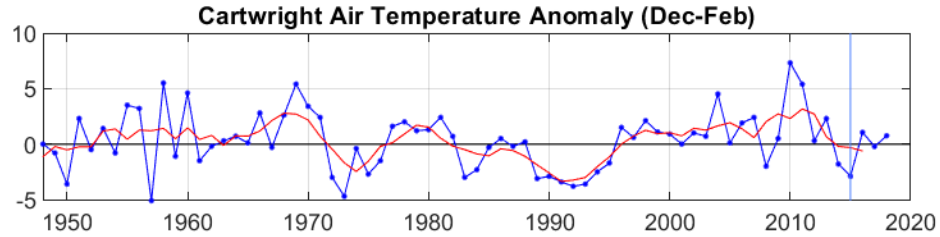
Cartwright Air Temperature Anomaly (Dec-Feb)
10
5
0
-5
1950
1960
1970
1980
1990
2000
2010
2020

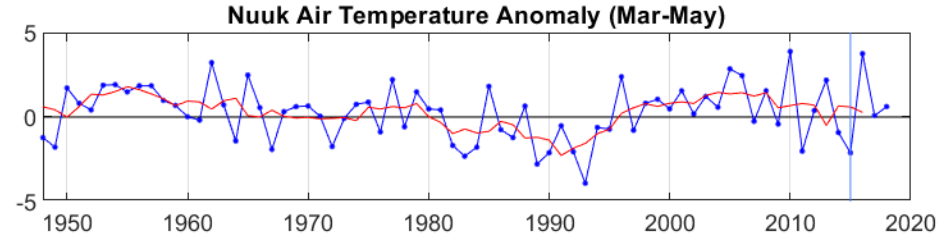
Nuuk Air Temperature Anomaly (Mar-May)
5
0
-5
1950
1960
1970
1980
1990
2000
2010
2020

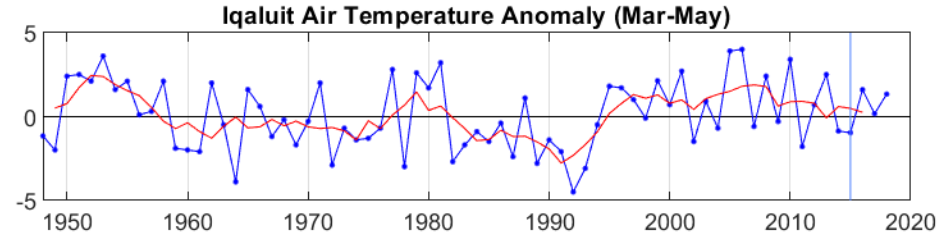
Iqaluit Air Temperature Anomaly (Mar-May)
5
0
-5
1950
1960
1970
1980
1990
2000
2010
2020

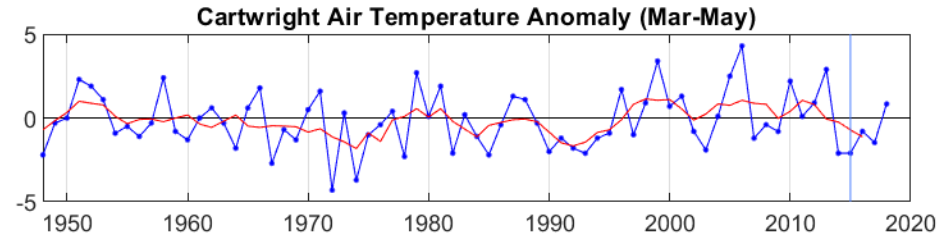
Cartwright Air Temperature Anomaly (Mar-May)
5
0
-5
1950
1960
1970
1980
1990
2000
2010
2020

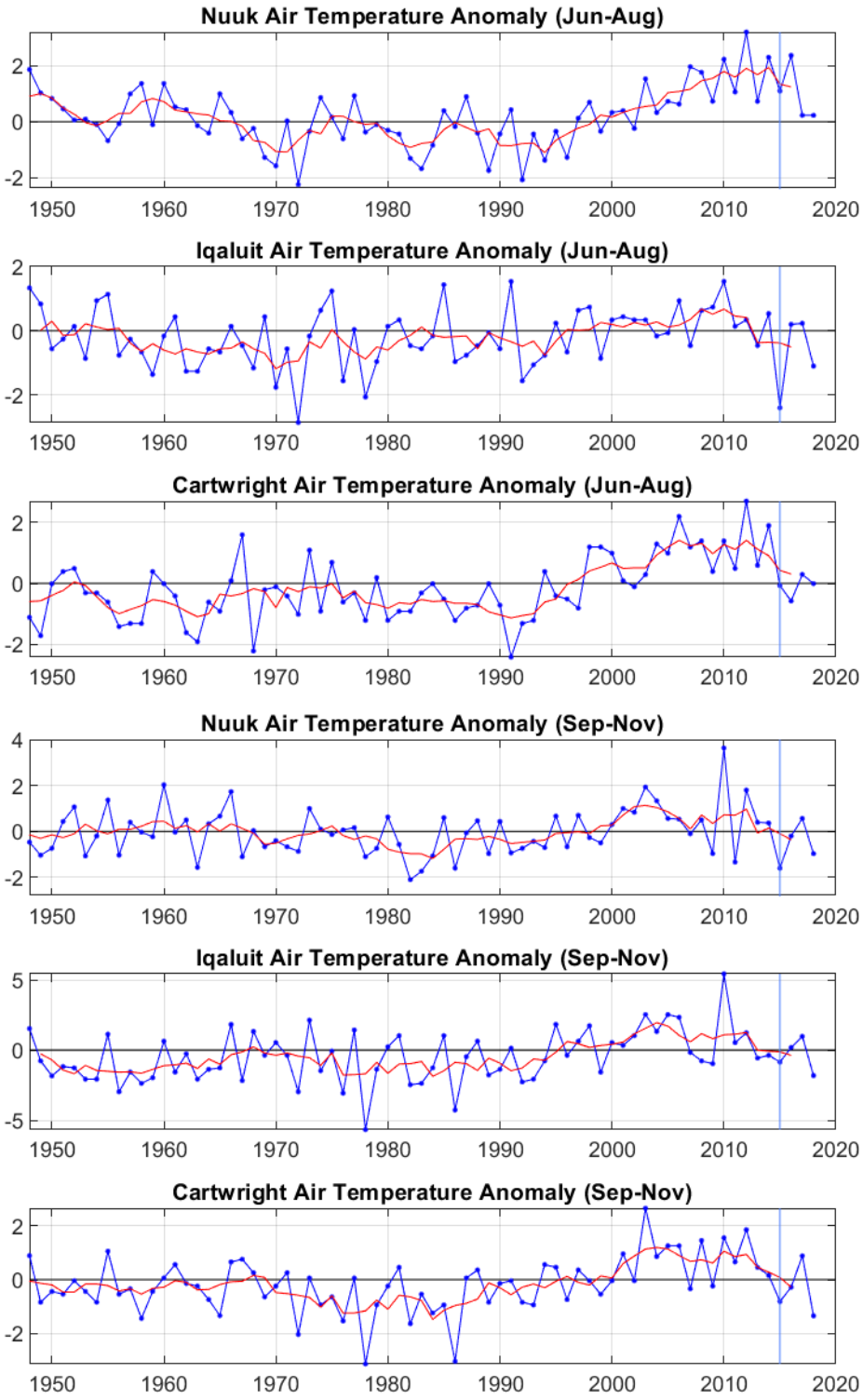

Figure 6. Seasonal air temperature anomalies averaged over winter (Dec-Feb), spring (Mar-May), summer (Jun-Aug) and fall (Sep-Nov) periods from 1948 to 2018. (blue) and their five year running means (red) for Nuuk, *Greenland*; Iqaluit, *Nunavut*; and Cartwright, *Labrador*.

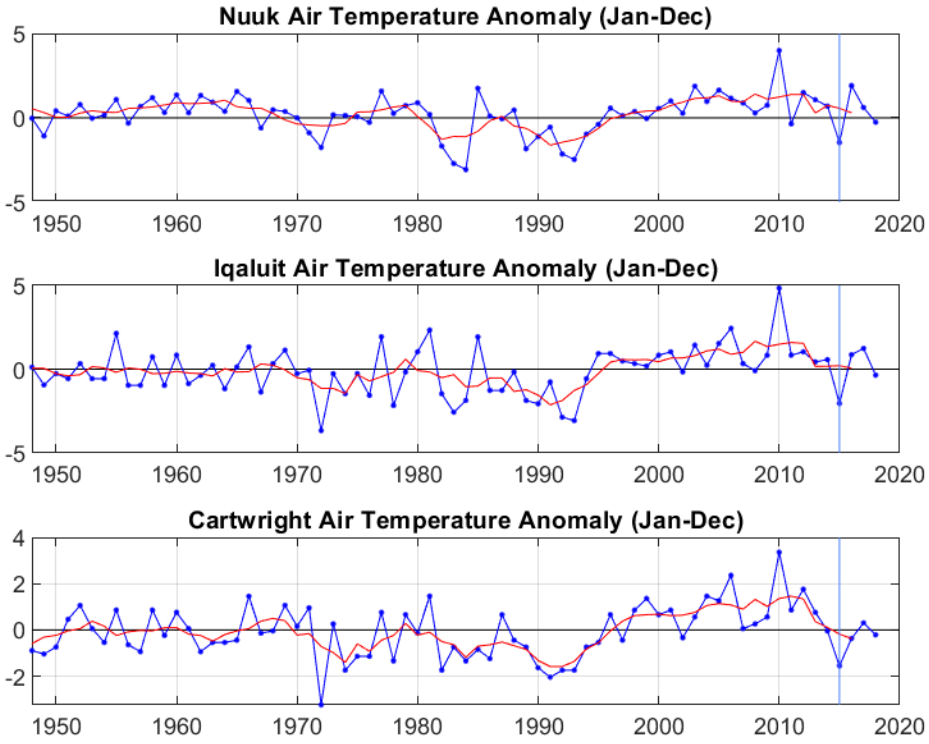

Figure 7. Annual air temperature anomalies (blue) and their five year running means (red) for: (1) Nuuk, Greenland (2) Iqaluit, Nunavut, and (3) Cartwright, Labrador.

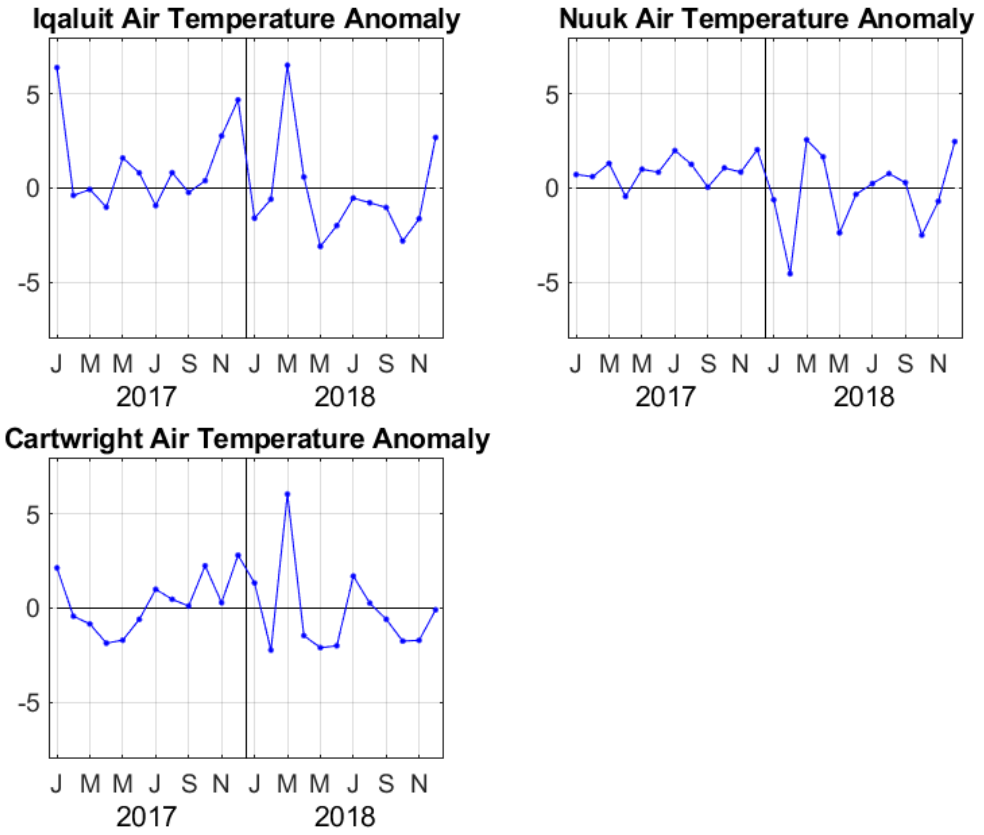

Figure 8. Monthly air temperature anomalies in 2017-2018 for: (1) Iqaluit, Nunavut, (2) Nuuk, Greenland, and (3) Cartwright, Labrador.

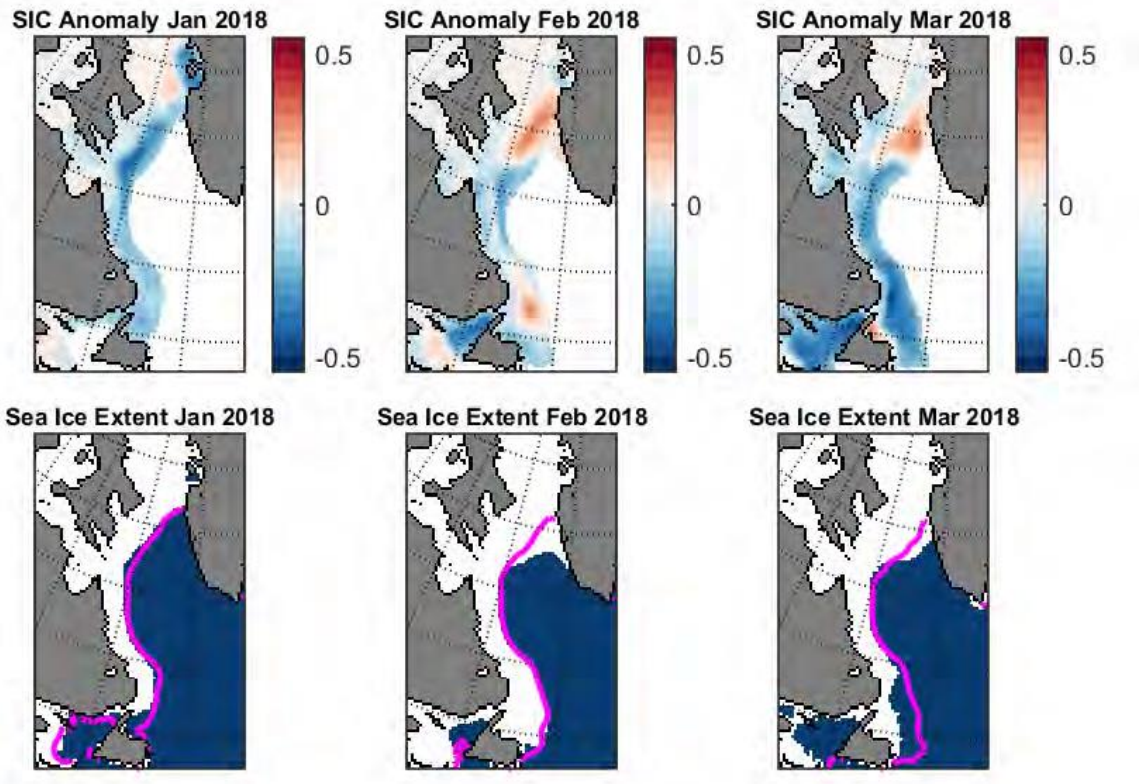

Figure 9. Sea ice concentration anomalies (top) and sea ice extent (bottom) for January-March 2018 as derived by the US National Snow and Ice Data Center (reference period 1979-2000) http://nsidc.org/.

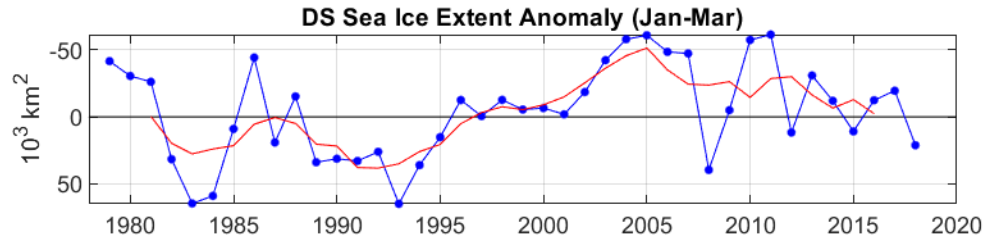
DS Sea Ice Extent Anomaly (Jan-Mar)
10^3 km^2
-50
0
50
1980
1985
1990
1995
2000
2005
2010
2015
2020

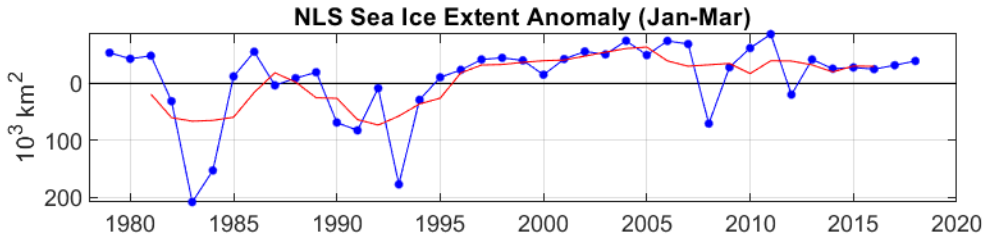
NLS Sea Ice Extent Anomaly (Jan-Mar)
10^3 km^2
0
100
200
1980
1985
1990
1995
2000
2005
2010
2015
2020

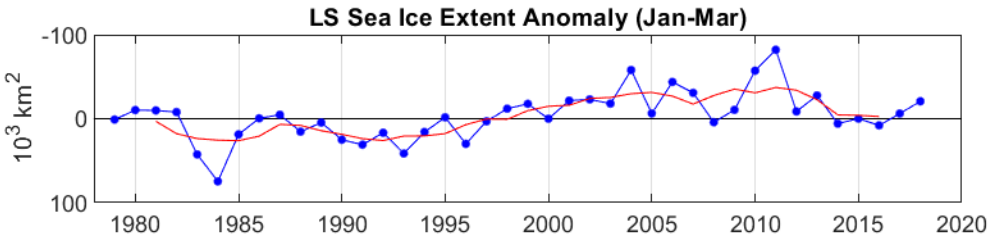
LS Sea Ice Extent Anomaly (Jan-Mar)
10^3 km^2
-100
0
100
1980
1985
1990
1995
2000
2005
2010
2015
2020

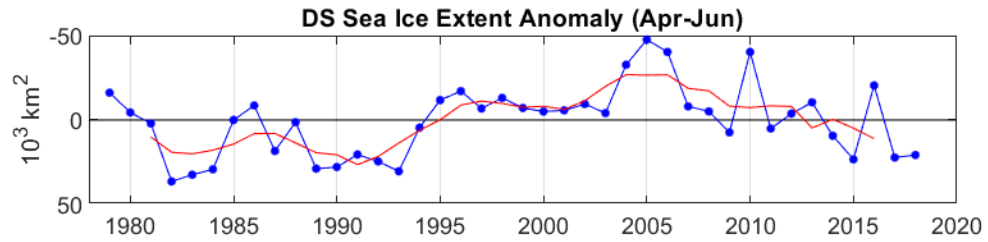
DS Sea Ice Extent Anomaly (Apr-Jun)
10^3 km^2
-50
0
50
1980
1985
1990
1995
2000
2005
2010
2015
2020

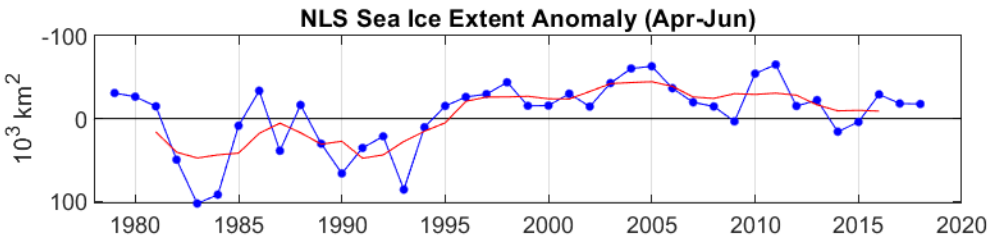
NLS Sea Ice Extent Anomaly (Apr-Jun)
10^3 km^2
-100
0
100
1980
1985
1990
1995
2000
2005
2010
2015
2020

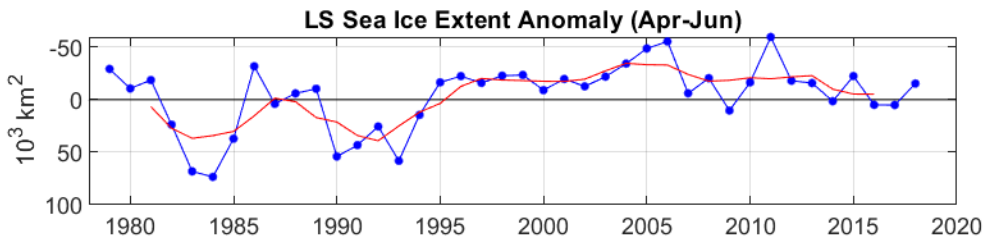
LS Sea Ice Extent Anomaly (Apr-Jun)
10^3 km^2
-50
0
50
100
1980
1985
1990
1995
2000
2005
2010
2015
2020

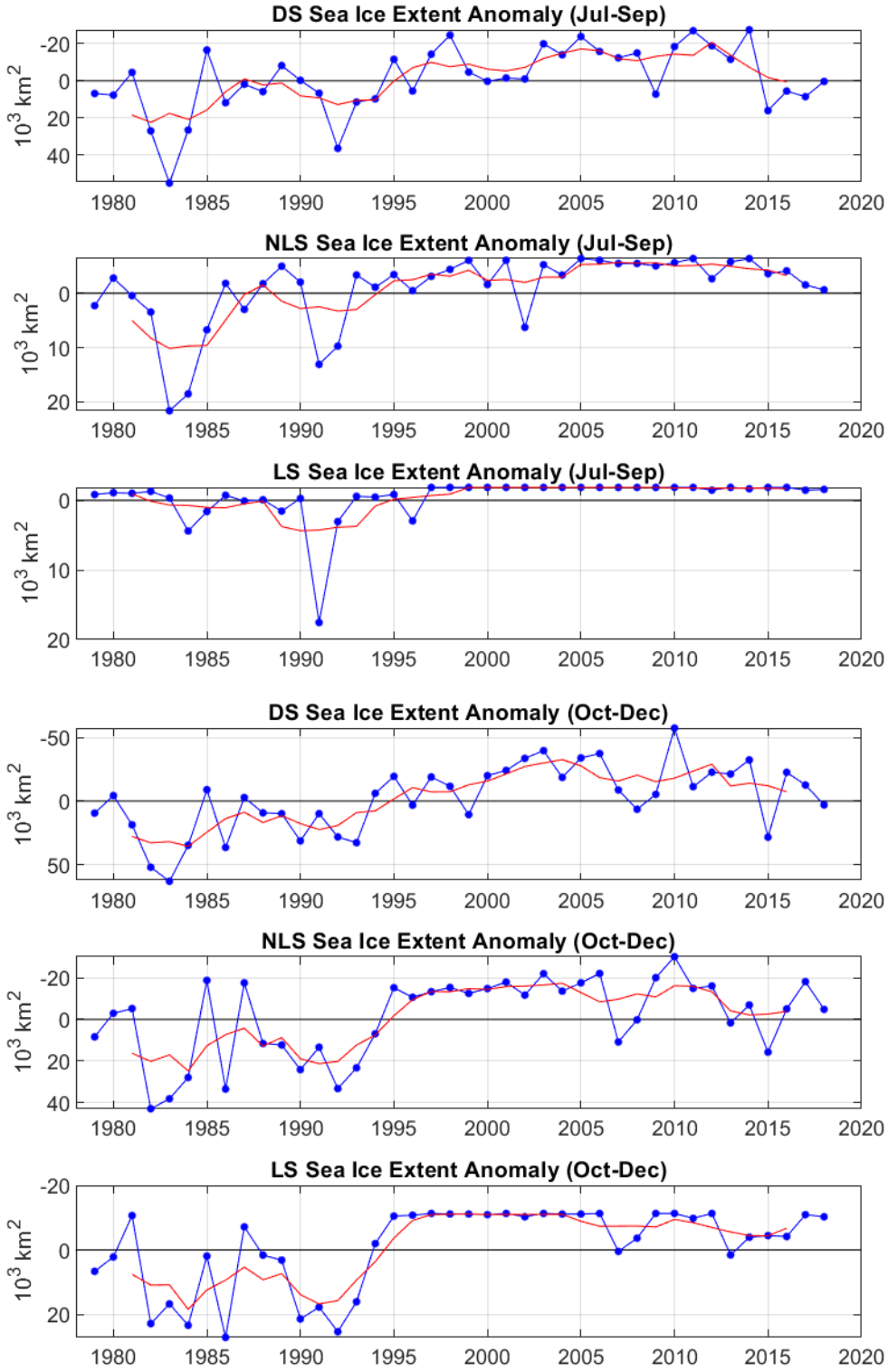

Figure 10. Seasonal sea ice extent anomalies (blue) and their five year running means (red) for: (1) Davis Strait (63-68°N), (2) the Northern Labrador Sea (58-63°N), and (3) Labrador Shelf (53-58°N).

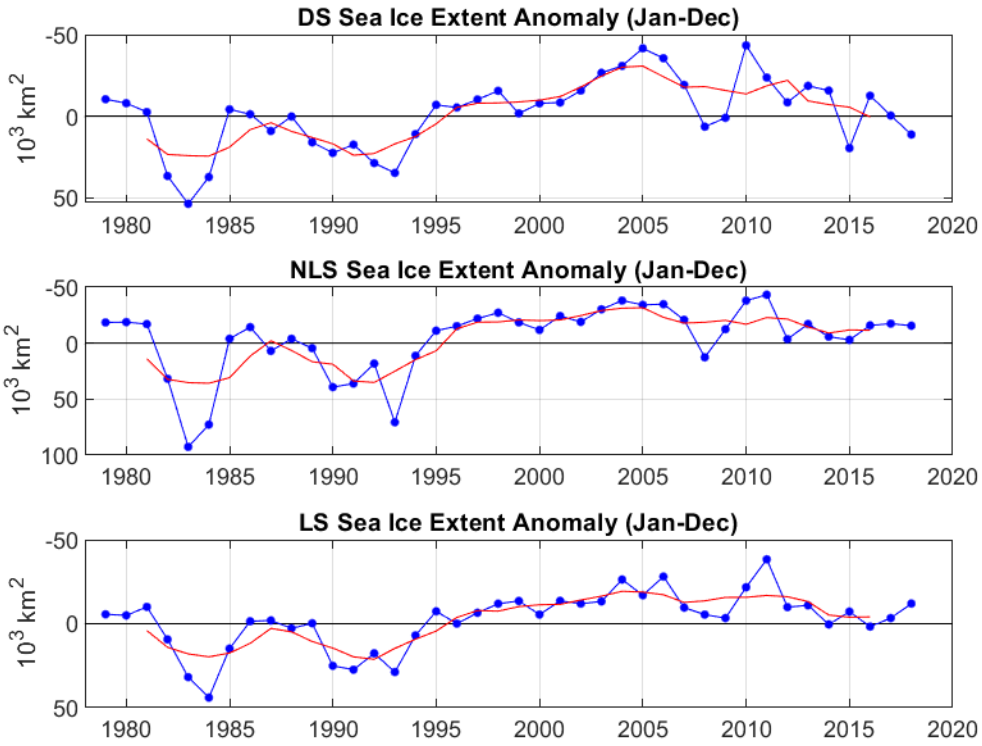

Figure 11. Annual sea ice extent anomalies (blue) and their five year running means (red) for: (1) Davis Strait (63-68°N), (2) the Northern Labrador Sea (58-63°N), and (3) Labrador Shelf (53-58°N).

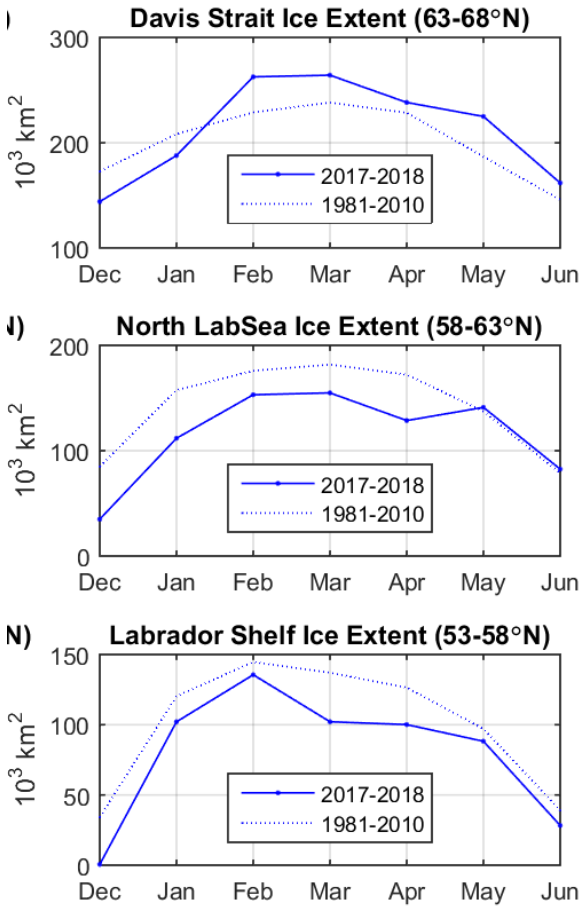

Figure 12. Monthly mean sea ice extent for December 2017 to June 2018 (solid line) and 1981-2010 mean monthly sea ice extent (dotted line) for (1) Davis Strait (63-68°N), (2) the Northern Labrador Sea (58-63°N), and (3) Labrador Shelf (53-58°N). These series are based on ice concentration data from the US National Snow and Ice Data Center (reference period 1981-2010). http://nsidc.org/data/ .

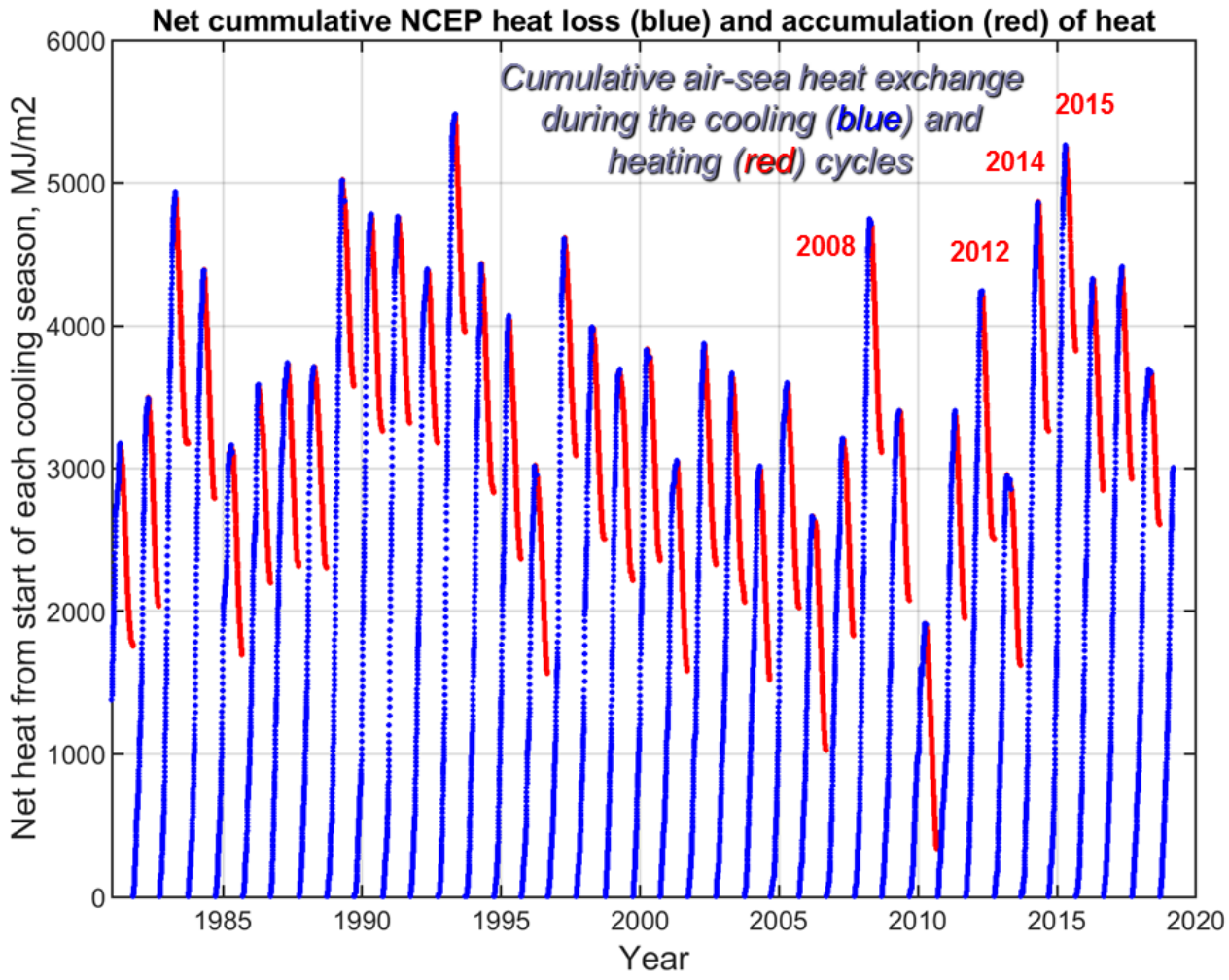

Figure 13. Sea surface heat losses/gains (blue/red) integrated over individual cooling/heating seasons in the central region Labrador Sea. The net heat flux values unsed in this intergration were computed as a sum of incoming and outgoing short and long wave readiation, latent and sinsible heat fluxes based on the NCEP/NCAR reanalysis fields. The years of high surface heat losses recorded in the Labrador Sea over the past ten years are indicated with red circles.

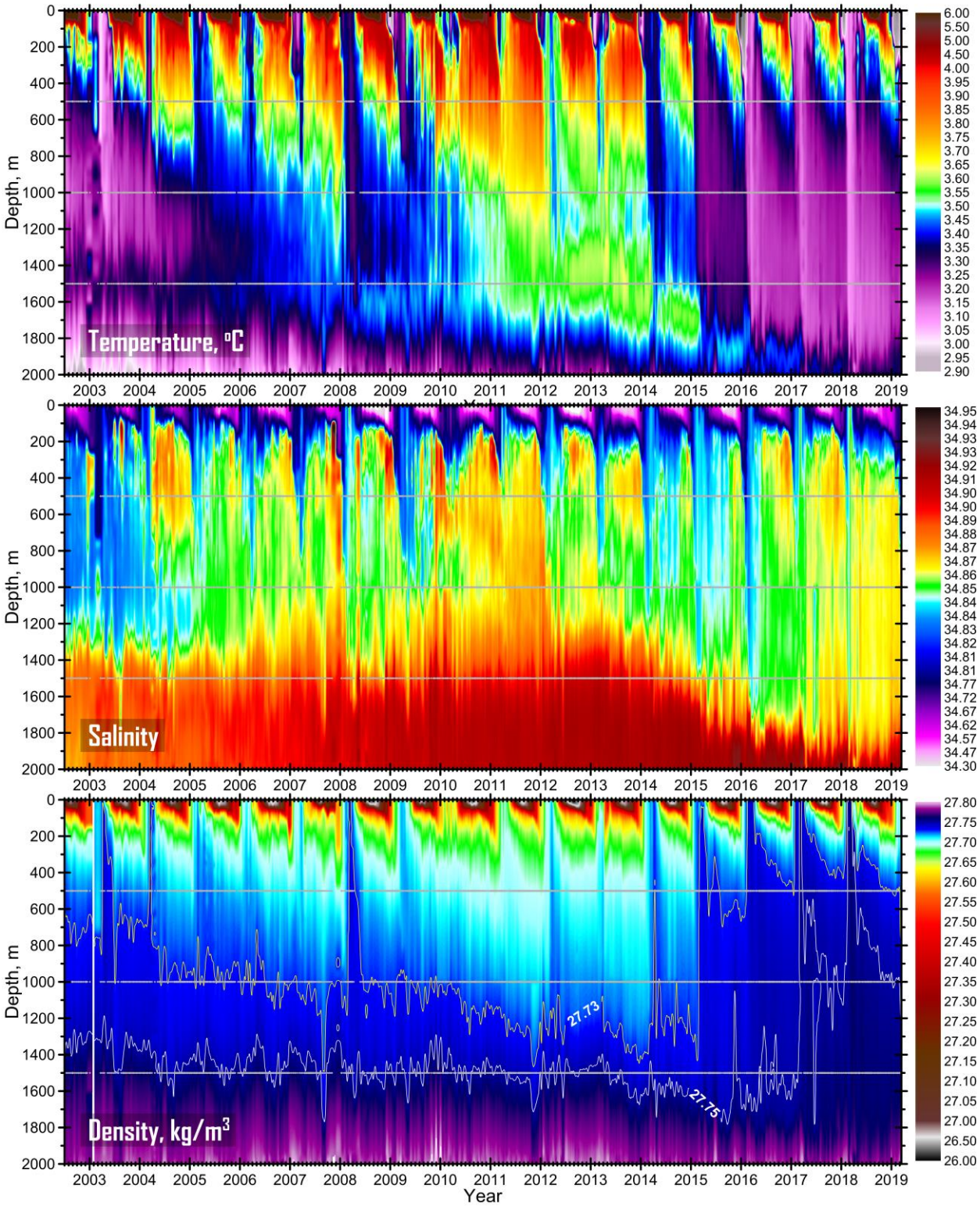

Figure 14. Variability of temperature (upper panel), salinity (lower panel) and density (lower panel) in the central region of the Labrador Sea based on profiling Argo float and research vessel survey data from 0 to 2000 m for the time period of 2002-2019.

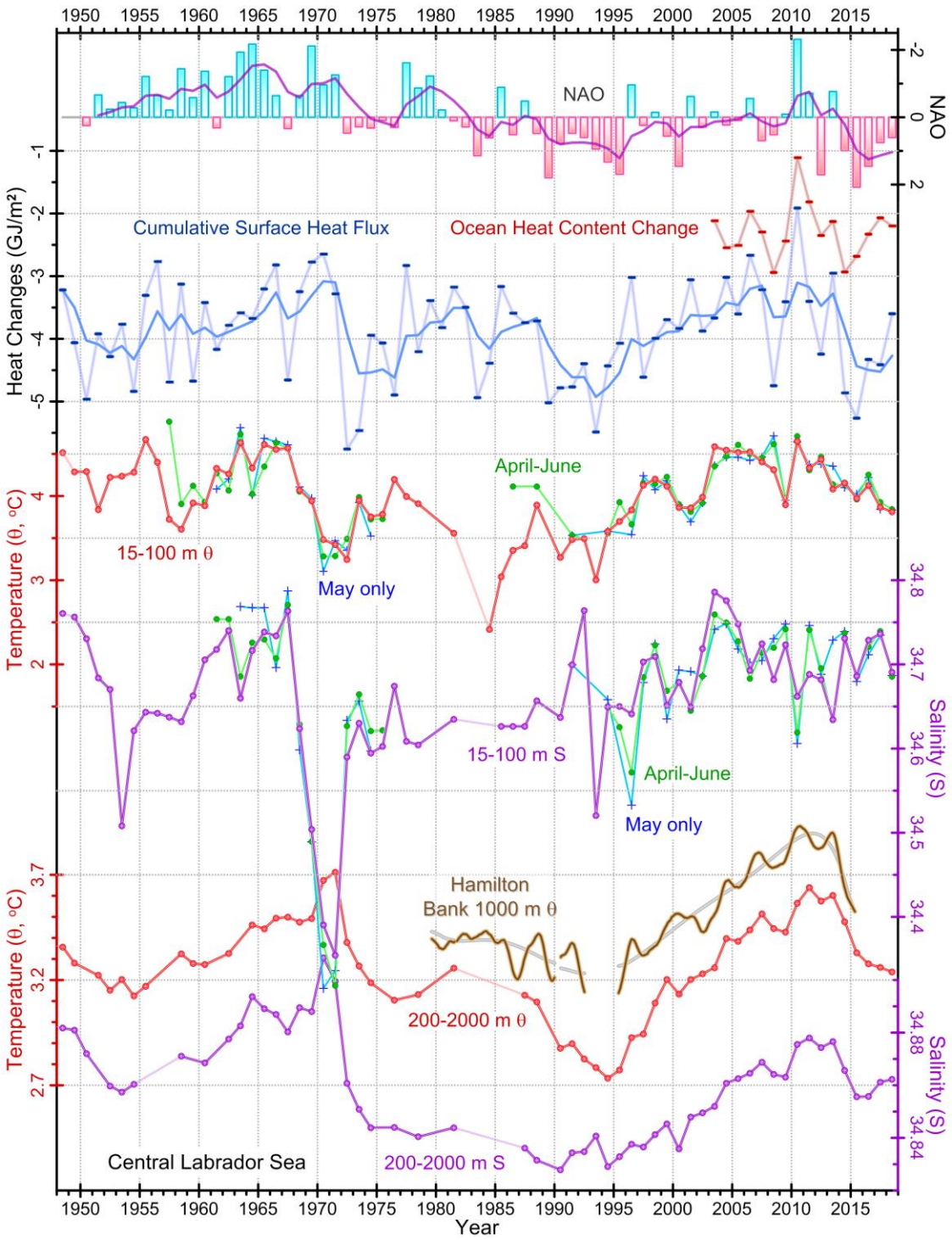

Figure 15. Labrador Sea indices since 1948. From top down: the normalized winter NAO index (upper bar graph, inverted scale); the central Labrador Sea: the change in the ocean's heat content during each annual cooling season of the Argo era (red), and the cumulative surface heat flux computed from NCEP data (blue), solid lines indicate five-back-point filtered series; annual, spring and May mean temperature (θ) and salinity (S) averaged over the 15-100 m depth range, annual mean θ and S averaged over the 200–2000 m range in the central Labrador Sea, and temperature from near-bottom current meter at about/approximately 1000 m depth east of Hamilton Bank.

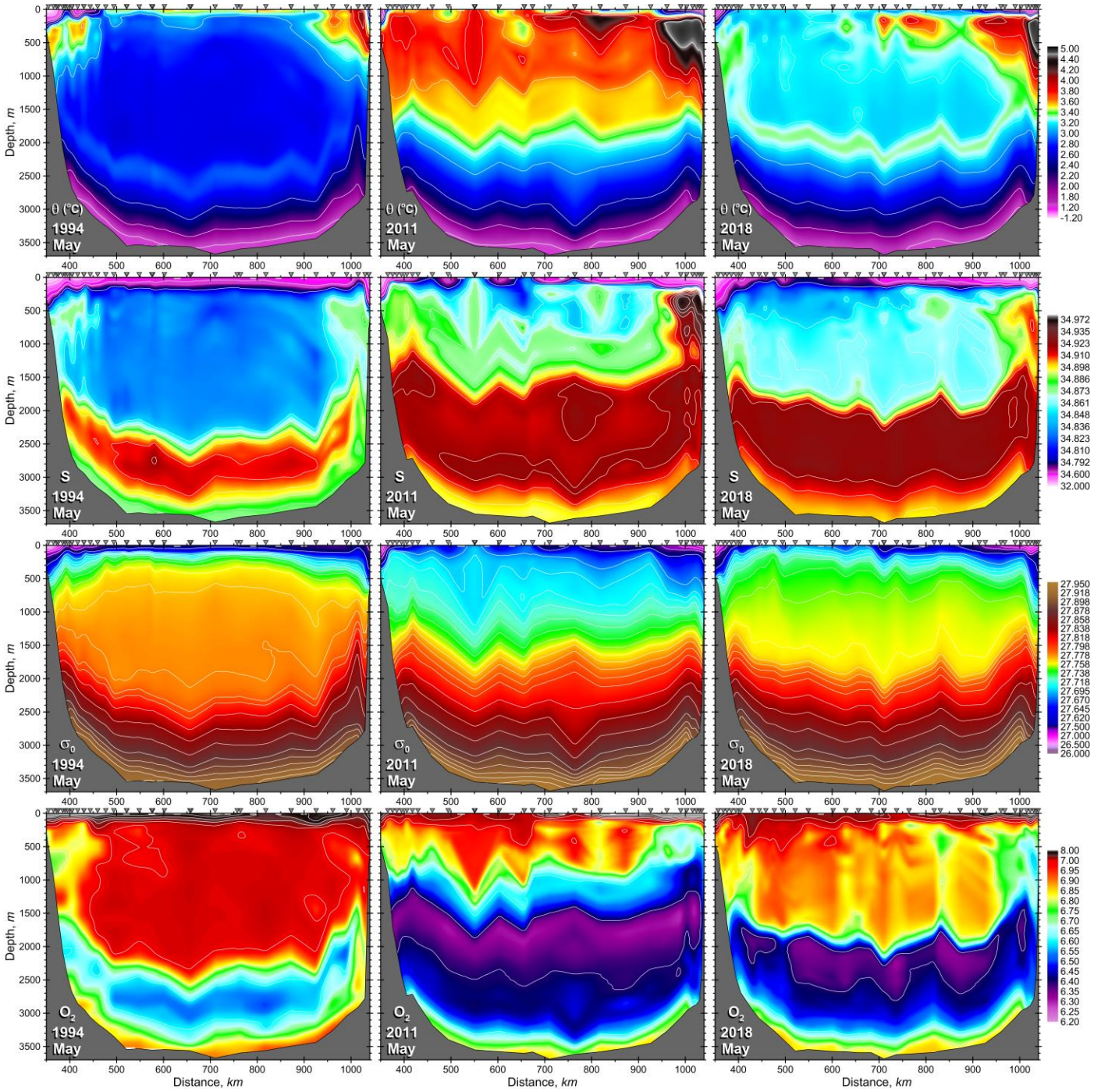

Figure 16. Distributions of potential temperature (θ, °C), salinity (S), potential density (σ_o, referenced to the surface, kg/m^3) and dissolved oxygen (ml/l) on the AR7W line across the Labrador Sea from annual spring-summer surveys in 1994, 2011 and 2018. Inverted triangles along the top of each panel indicate station locations.

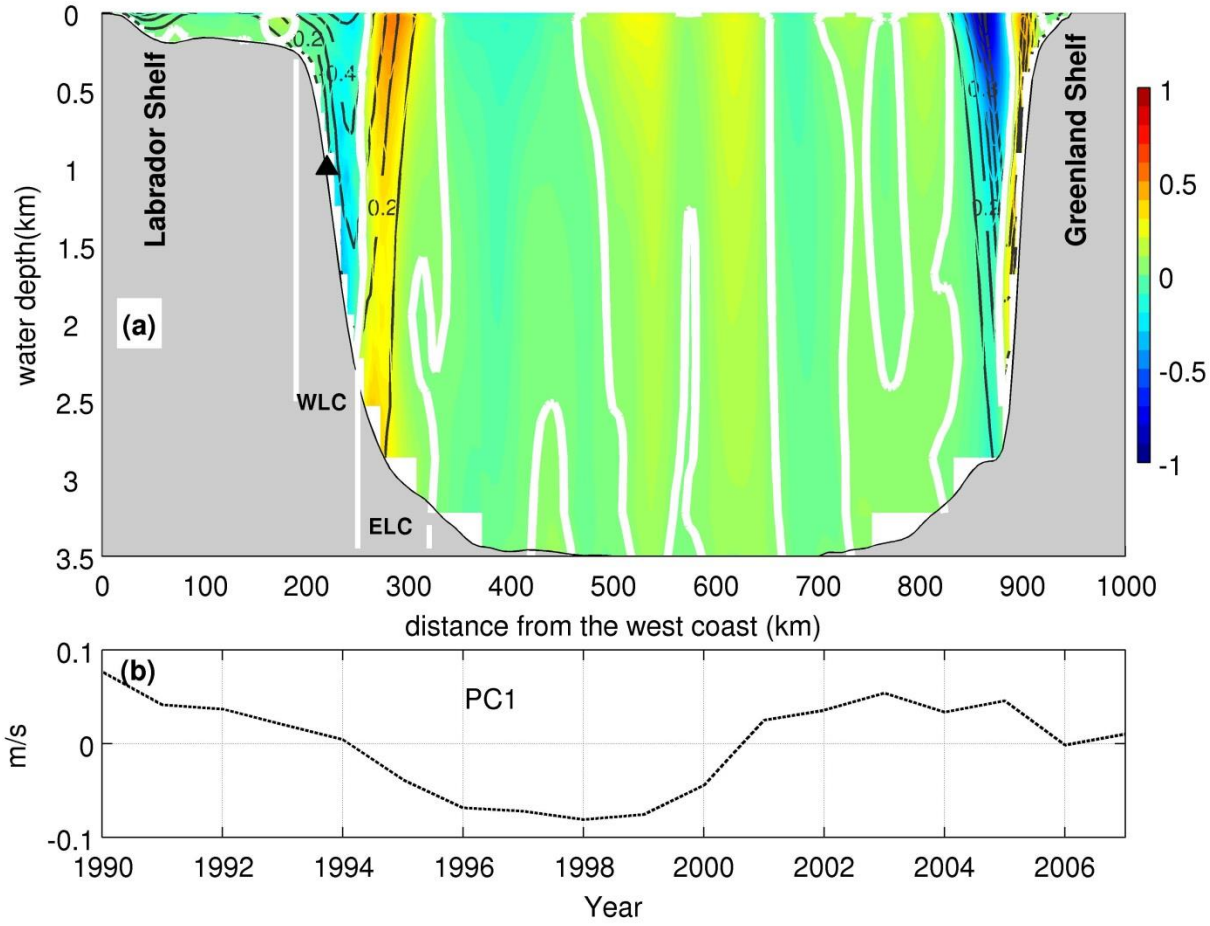

Figure 17. (a) EOF1 pattern of the normal velocities along AR7W (based on results from 1990 to 2007). The shaded areas represent the EOF pattern, bold white lines are zeros contours of the EOF pattern, the black labeled lines are the mean normal velocities (in m/s). Note: positive direction is northward. The black triangle indicates the location of the mooring referred to in the text. (b) Corresponding PC1.

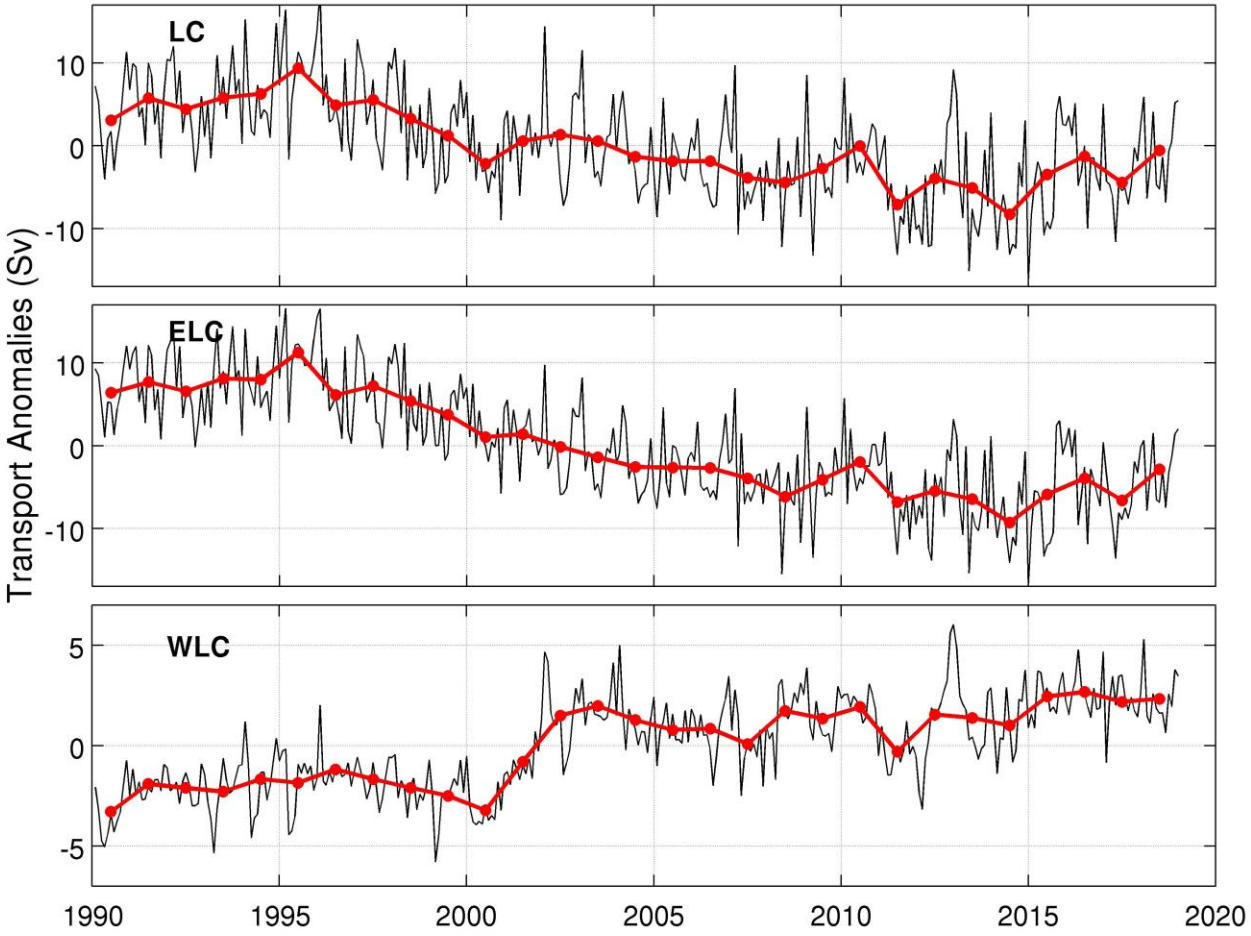

Figure 18. Transport anomalies of the LC, ELC, and WLC from 1990 to 2018. Note: black lines are from the monthly data, and red lines and dots are from the annual means.

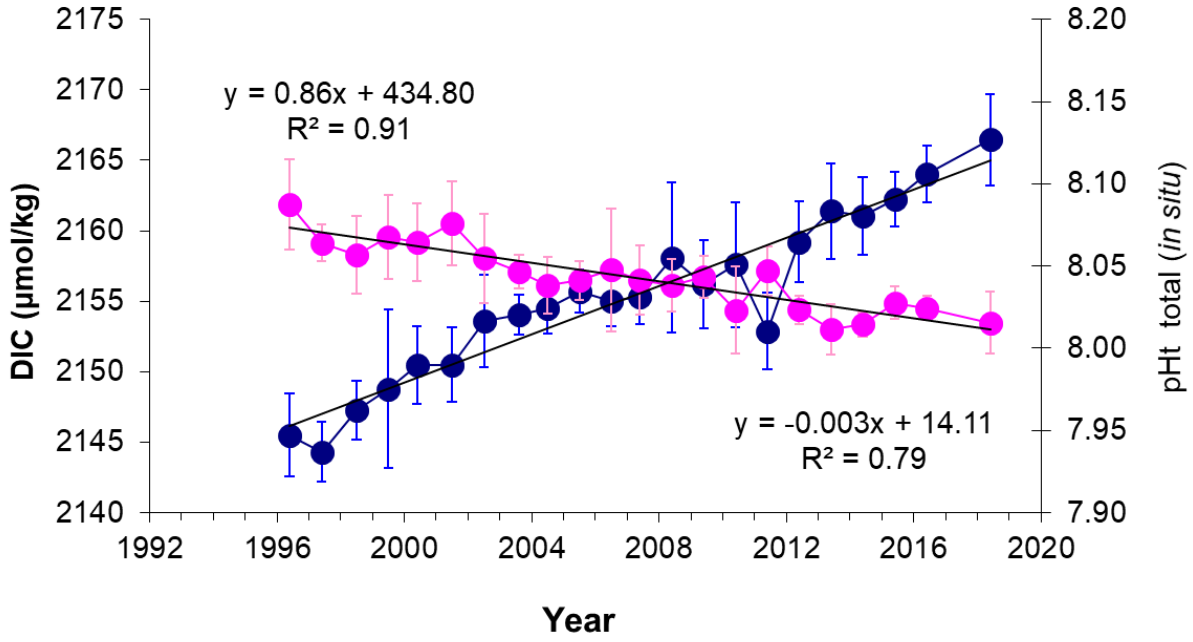

Figure 19. Time series of total inorganic carbon (DIC) in blue and pH in pink in the 150-500 m depth layer in the central Labrador Sea. Corresponding regression lines for stations located in the Labrador Basin for the period 1996–2018.

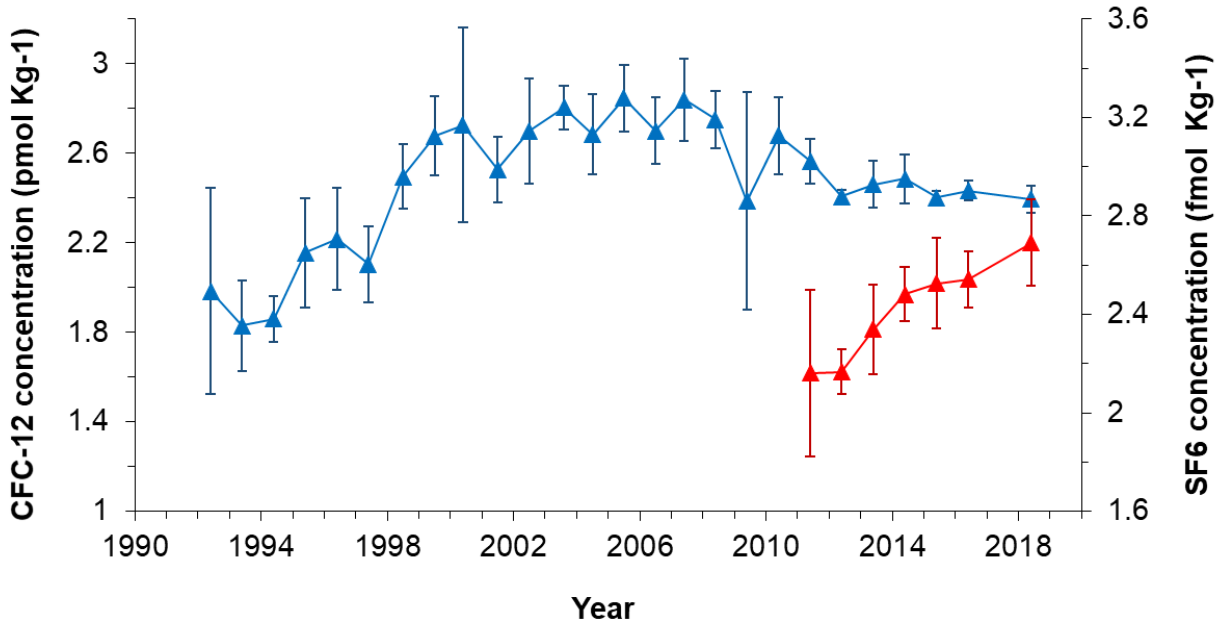

Figure 20. Annual mean concentrations of CFC-12 (blue) and SF_6 (red) in the vertical layer confined to 150-500 m in the central part of the Labrador Sea Basin from 1991 to 2018. SF_6 measurements only began in 2011.

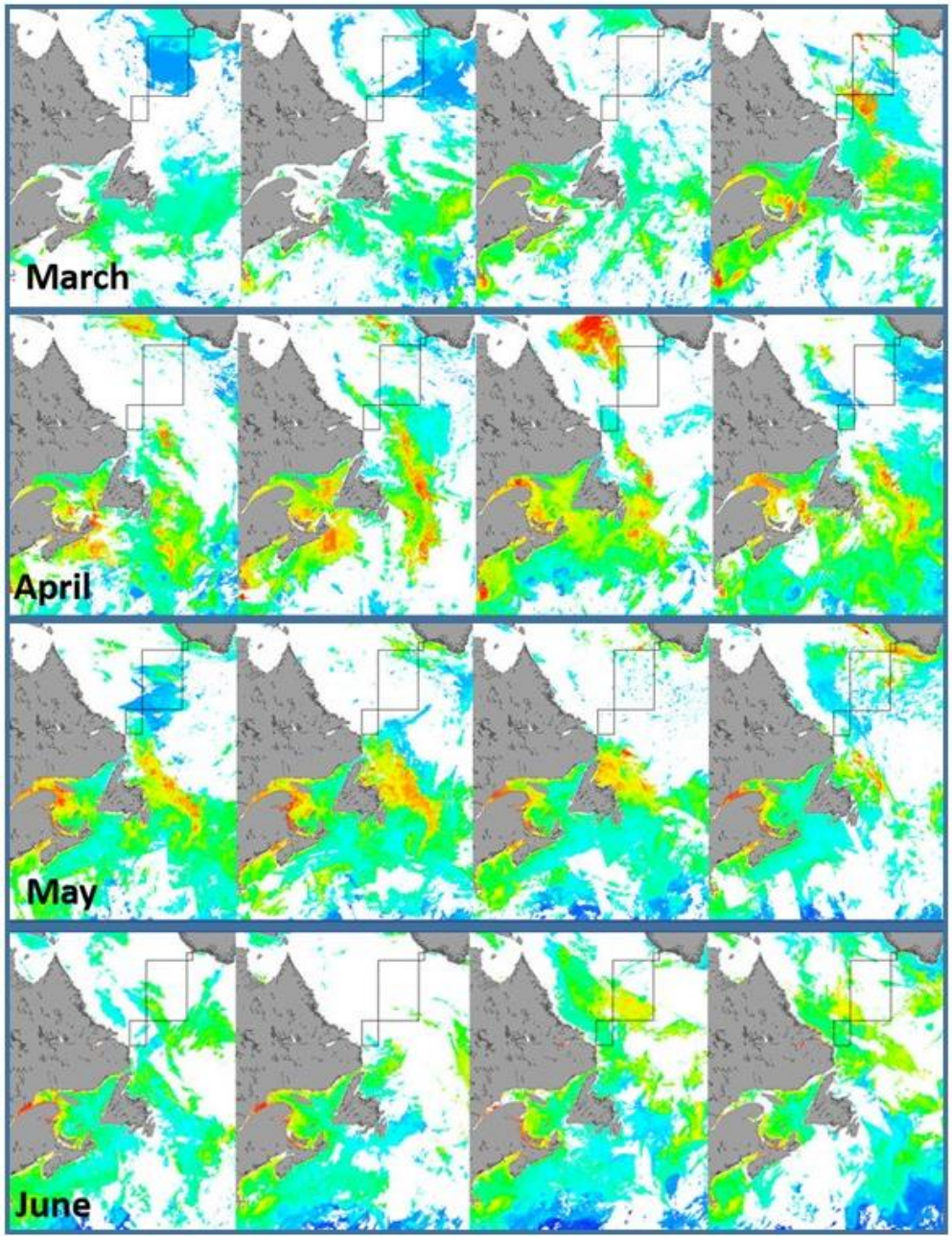

Figure 21. Weekly VIIRS ocean colour composite 2018 April to June for the Northwest Atlantic region. The black boxes indicate the Labrador Shelf/Slope (LS/S), Labrador Basin (LB) and Greenland Shelf/slope (GS/S) regions used for the averaging of remote-sensed data presented a longer term time the time series as present in Figure 22.

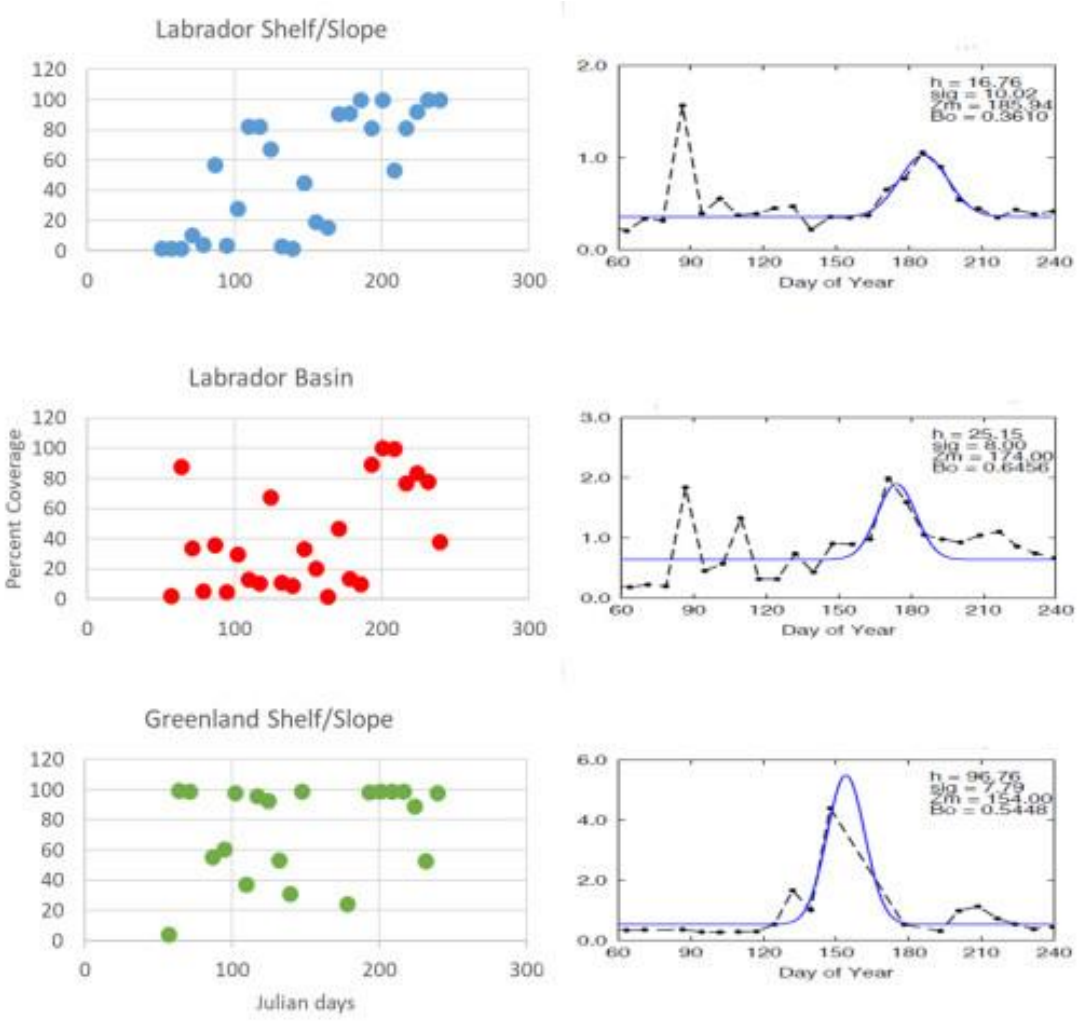

Figure 22. Percent weekly coverage for each of the region of Interest are shown on the left panels with LS/S, LB and GS/S respectively from top to bottom. On the right are the phytoplankton bloom characterisation (dashed line) using fitted Gaussian curve (hard blue line) used to define the bloom characteristics following (Zhai et al., 1991).

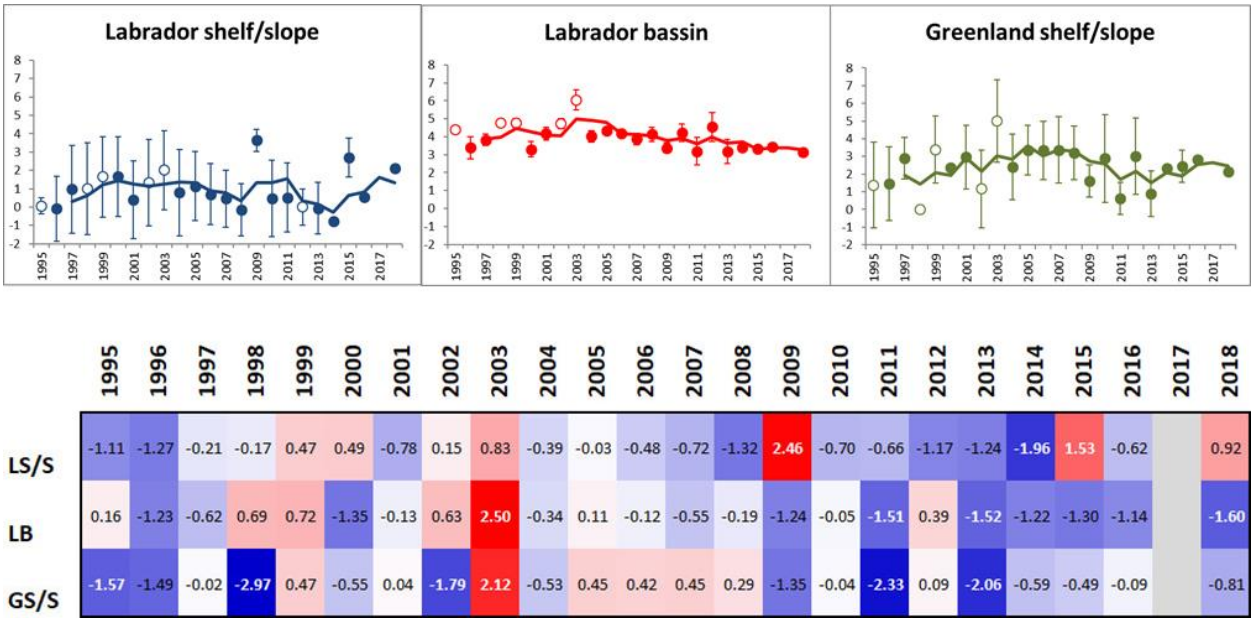

Figure 23. Water temperature averaged between the surface and 100 m and by regions. The top row panels represent the average values by regions where the Shelf/Slope (LS/S) is in blue, the Labrador Basin (LB) is in green and Greenland Shelf/slope (GS/S) in red. Open circles designate years when the sampling occurred later in a year, in June-July. Additionally, the AR7W survey dates have recently shifted from the mid-end May to the early May. The changing year days of the ship survey add a strong seasonal bias to the values included in this figure and limit interpretation of the presented series. The bottom panel shows the same data expressed in normalized anomalies based on a 1999 to 2010 reference period.

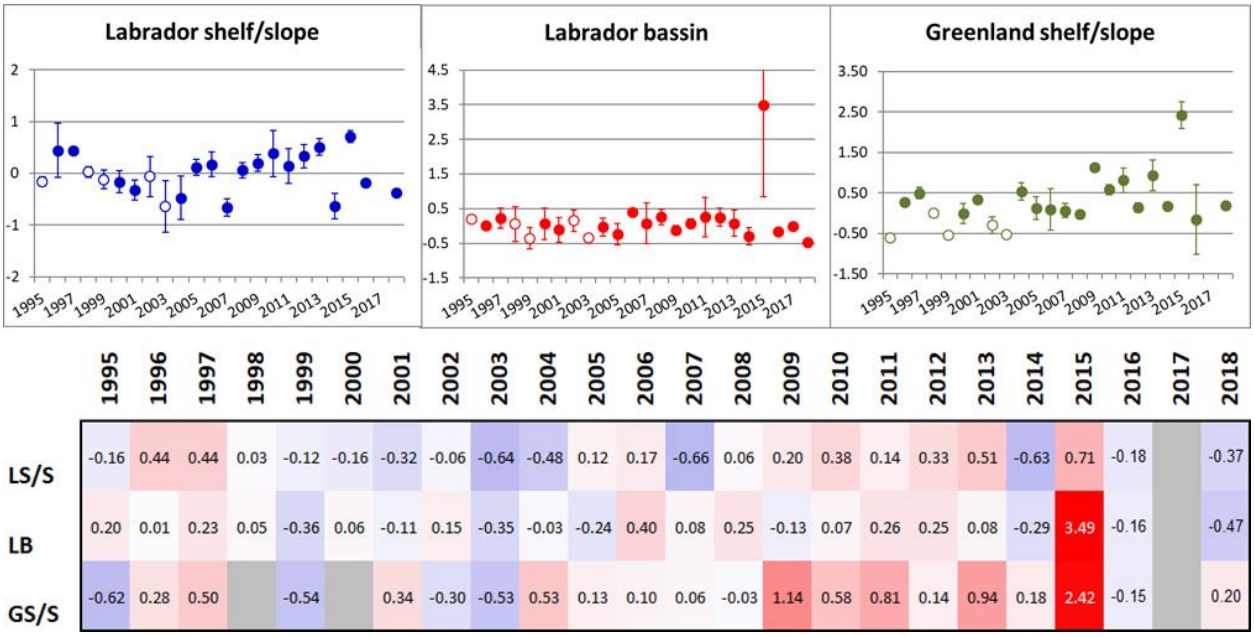

Figure 24. Chlorophyll-*a* integrated between the surface and 100 m and averaged by regions. The top row panels represent the average values by regions where the Shelf/Slope (LS/S) is in blue, the Labrador Basin (LB) is in green and Greenland Shelf/slope (GS/S) in red. Open circles designate years when the sampling occurred later in a year, in June-July. Additionally, the AR7W survey dates have recently shifted from the mid-end May to the early May. The changing year days of the ship survey add a strong seasonal bias to the values included in this figure and limit interpretation of the presented series. The bottom panel shows the same data expressed in normalized anomalies based on a 1999 to 2010 reference period.

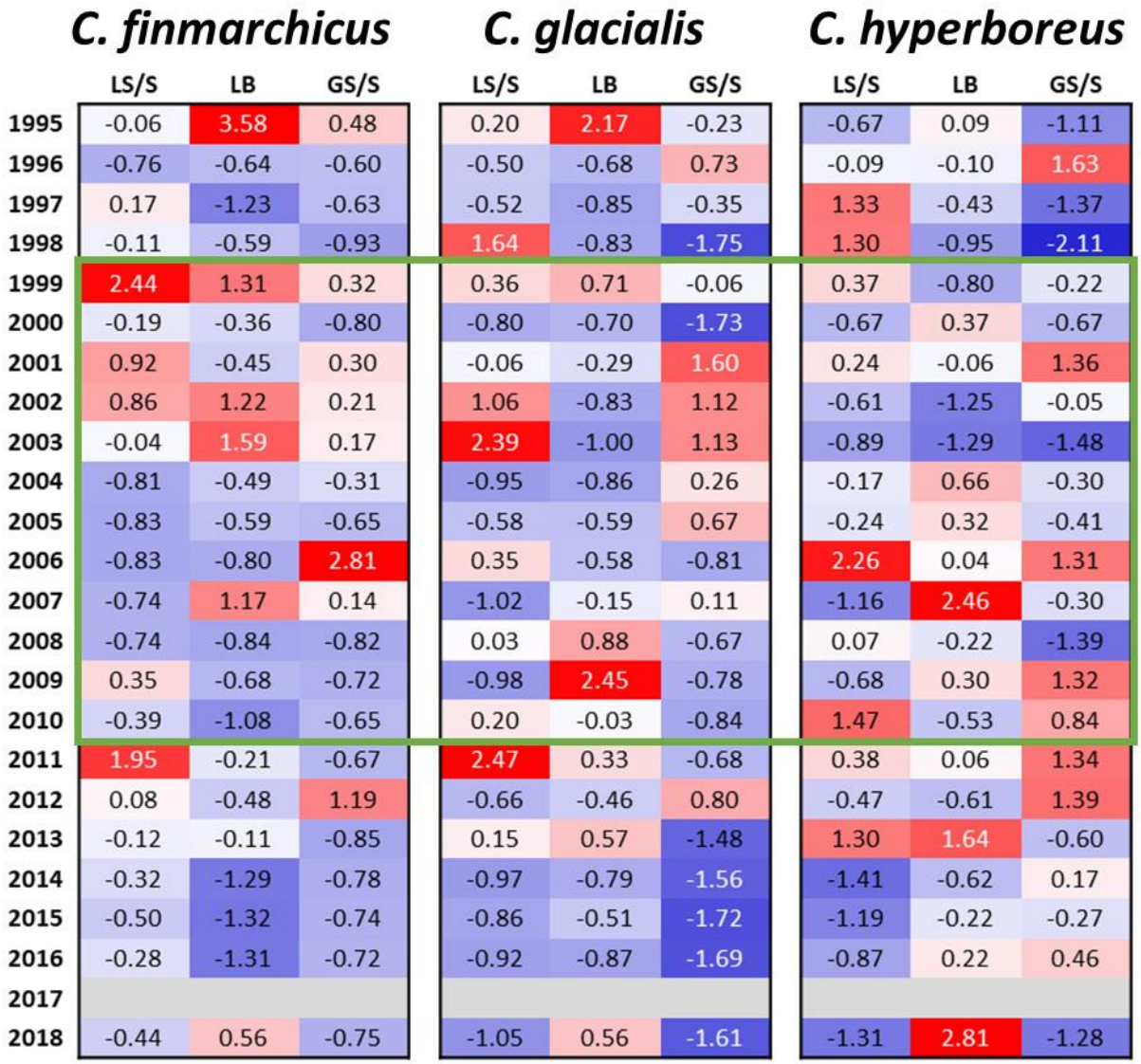

	C. finmarchicus			*C. glacialis*			*C. hyperboreus*		
	LS/S	LB	GS/S	LS/S	LB	GS/S	LS/S	LB	GS/S
1995	-0.06	3.58	0.48	0.20	2.17	-0.23	-0.67	0.09	-1.11
1996	-0.76	-0.64	-0.60	-0.50	-0.68	0.73	-0.09	-0.10	1.63
1997	0.17	-1.23	-0.63	-0.52	-0.85	-0.35	1.33	-0.43	-1.37
1998	-0.11	-0.59	-0.93	1.64	-0.83	-1.75	1.30	-0.95	-2.11
1999	2.44	1.31	0.32	0.36	0.71	-0.06	0.37	-0.80	-0.22
2000	-0.19	-0.36	-0.80	-0.80	-0.70	-1.73	-0.67	0.37	-0.67
2001	0.92	-0.45	0.30	-0.06	-0.29	1.60	0.24	-0.06	1.36
2002	0.86	1.22	0.21	1.06	-0.83	1.12	-0.61	-1.25	-0.05
2003	-0.04	1.59	0.17	2.39	-1.00	1.13	-0.89	-1.29	-1.48
2004	-0.81	-0.49	-0.31	-0.95	-0.86	0.26	-0.17	0.66	-0.30
2005	-0.83	-0.59	-0.65	-0.58	-0.59	0.67	-0.24	0.32	-0.41
2006	-0.83	-0.80	2.81	0.35	-0.58	-0.81	2.26	0.04	1.31
2007	-0.74	1.17	0.14	-1.02	-0.15	0.11	-1.16	2.46	-0.30
2008	-0.74	-0.84	-0.82	0.03	0.88	-0.67	0.07	-0.22	-1.39
2009	0.35	-0.68	-0.72	-0.98	2.45	-0.78	-0.68	0.30	1.32
2010	-0.39	-1.08	-0.65	0.20	-0.03	-0.84	1.47	-0.53	0.84
2011	1.95	-0.21	-0.67	2.47	0.33	-0.68	0.38	0.06	1.34
2012	0.08	-0.48	1.19	-0.66	-0.46	0.80	-0.47	-0.61	1.39
2013	-0.12	-0.11	-0.85	0.15	0.57	-1.48	1.30	1.64	-0.60
2014	-0.32	-1.29	-0.78	-0.97	-0.79	-1.56	-1.41	-0.62	0.17
2015	-0.50	-1.32	-0.74	-0.86	-0.51	-1.72	-1.19	-0.22	-0.27
2016	-0.28	-1.31	-0.72	-0.92	-0.87	-1.69	-0.87	0.22	0.46
2017									
2018	-0.44	0.56	-0.75	-1.05	0.56	-1.61	-1.31	2.81	-1.28

Figure 25. *Calanus finmarchicus*, *C. glacialis* and *C. hyperboreus* anomalies on abundance from 1995 to 2018 from the Labrador Shelf/Slope (LS/S), Labrador Basin (LB) and Greenland Shelf/slope (GS/S) regions. The green square represent the reference period running from 1999 to 2010. Open circles in Figures 23 an 24 designate years when the sampling occurred later in a year, in June-July. Additionally, the AR7W survey dates have recently shifted from the mid-end May to the early May. The changing year days of the ship survey can possibly add a seasonal bias affecting the values and limit interpretation of the presented material.

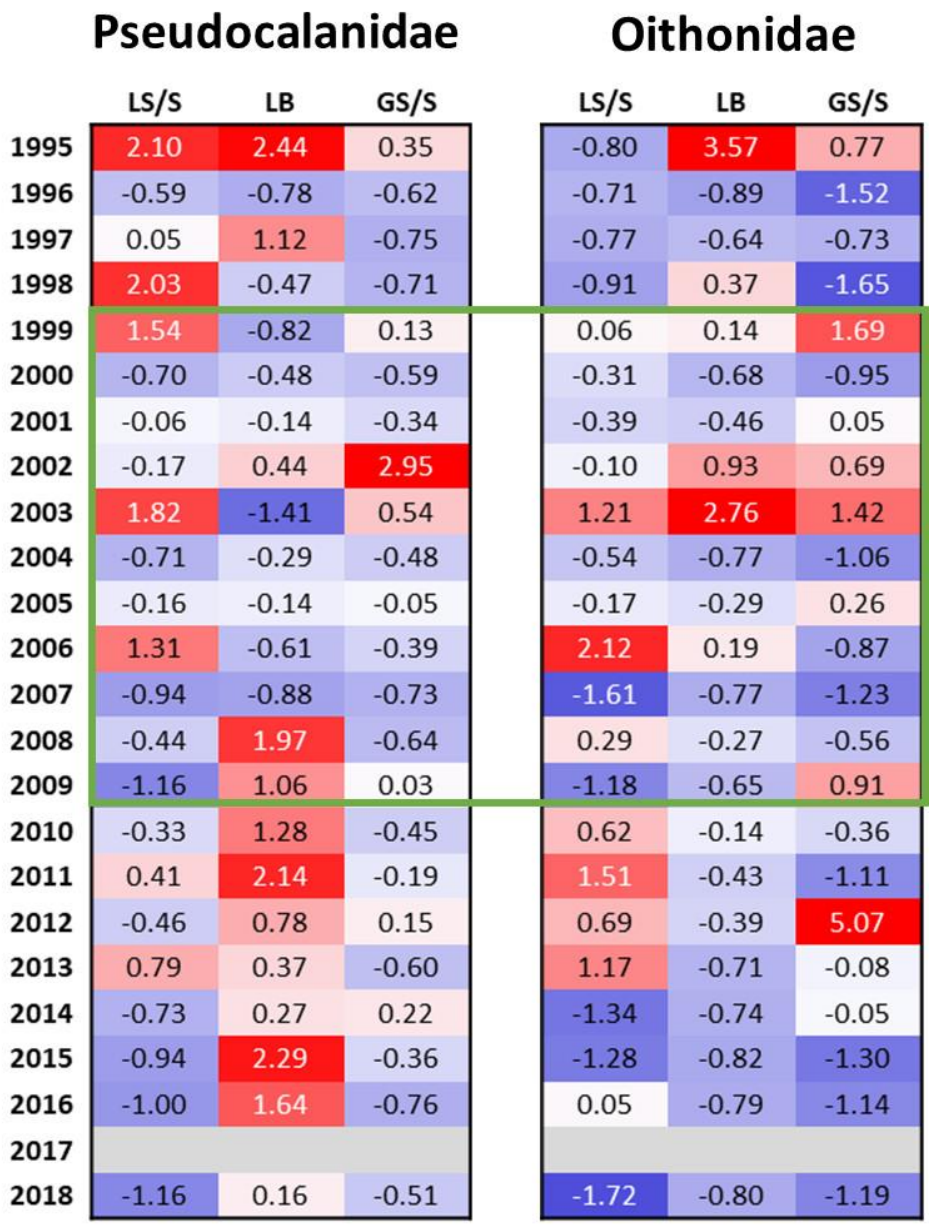

Figure 26. *Pseudocalanus* spp. and *Oithona* spp. anomalies on abundance from 1995 to 2018 from the Labrador Shelf/Slope (LS/S), Labrador Basin (LB) and Greenland Shelf/slope (GS/S) regions. The green square represent the reference period running from 1999 to 2010. Open circles in Figures 23 an 24 designate years when the sampling occurred later in a year, in June-July. Additionally, the AR7W survey dates have recently shifted from the mid-end May to the early May. The changing year days of the ship survey can possibly add a seasonal bias affecting the values and limit interpretation of the presented material.

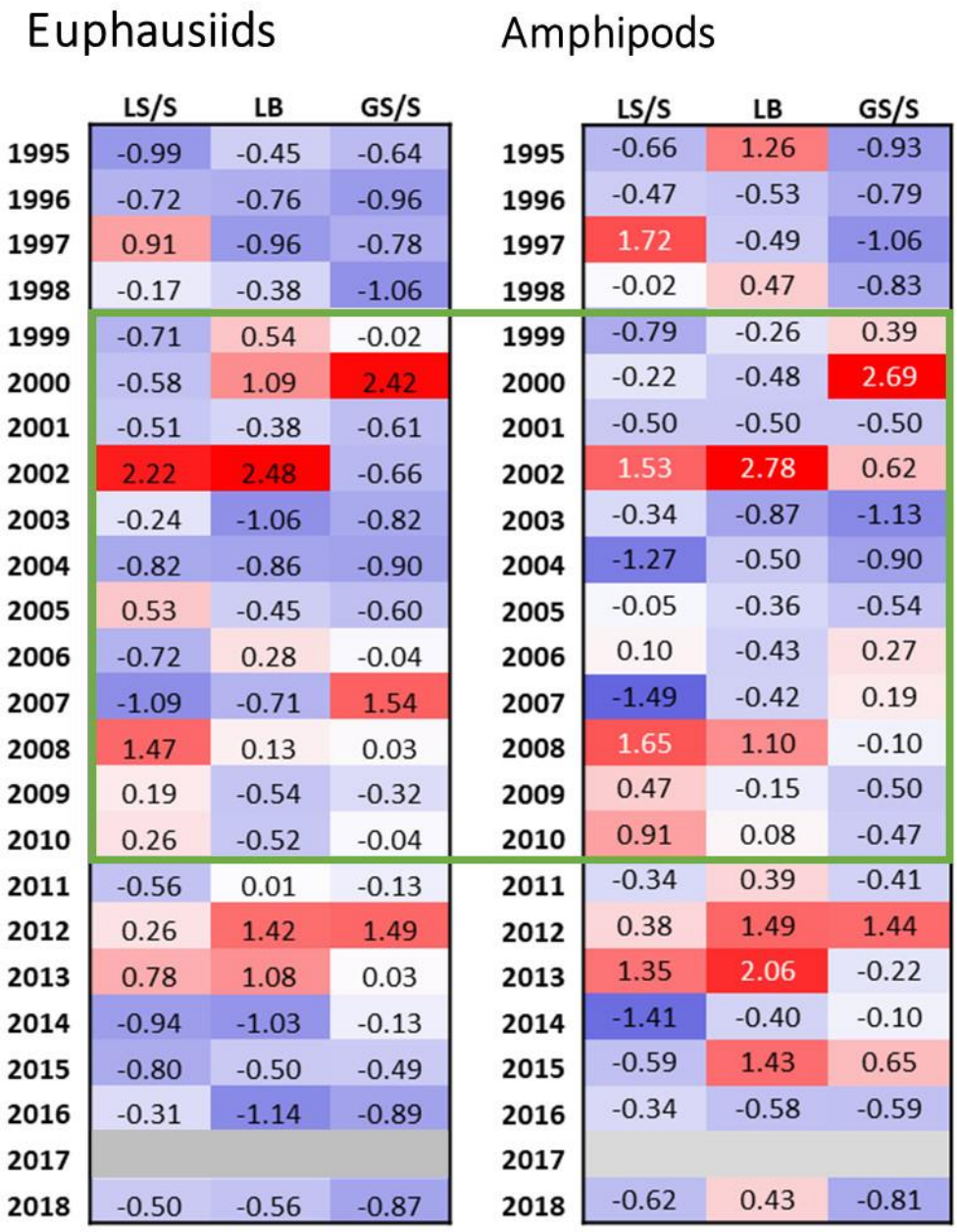

Figure 27. *Euphausiid* and *Hyperiid (Amphipode)* anomalies on abundance from 1995 to 2018 from the Labrador Shelf/Slope (LS/S), Labrador Basin (LB) and Greenland Shelf/slope (GS/S) regions. The green square represent the reference period running from 1999 to 2010. Open circles in Figures 23 an 24 designate years when the sampling occurred later in a year, in June-July. Additionally, the AR7W survey dates have recently shifted from the mid-end May to the early May. The changing year days of the ship survey can possibly add a seasonal bias affecting the values and limit interpretation of the presented material.

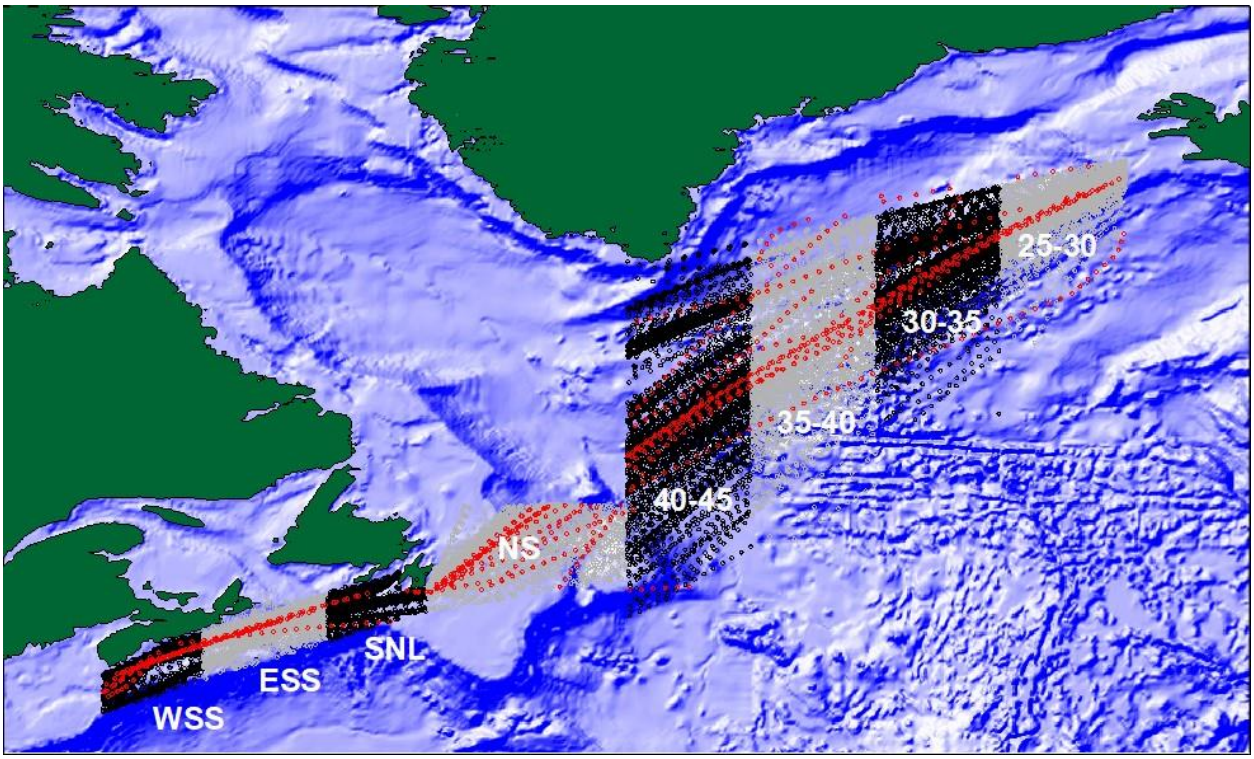

Figure 28. Continuous Plankton recorder (CPR) lines and stations 1957 to 2017. Stations sampled in 2017 are shown in red. Data are analysed by region. Regions are: Western Scotian Shelf (WSS), Eastern Scotian Shelf (ESS), South Newfoundland Shelf (SNL), Newfoundland Shelf (NS), and between longitudes 40-45°W, 35-40°W, 30-35°W, 25-30°W.

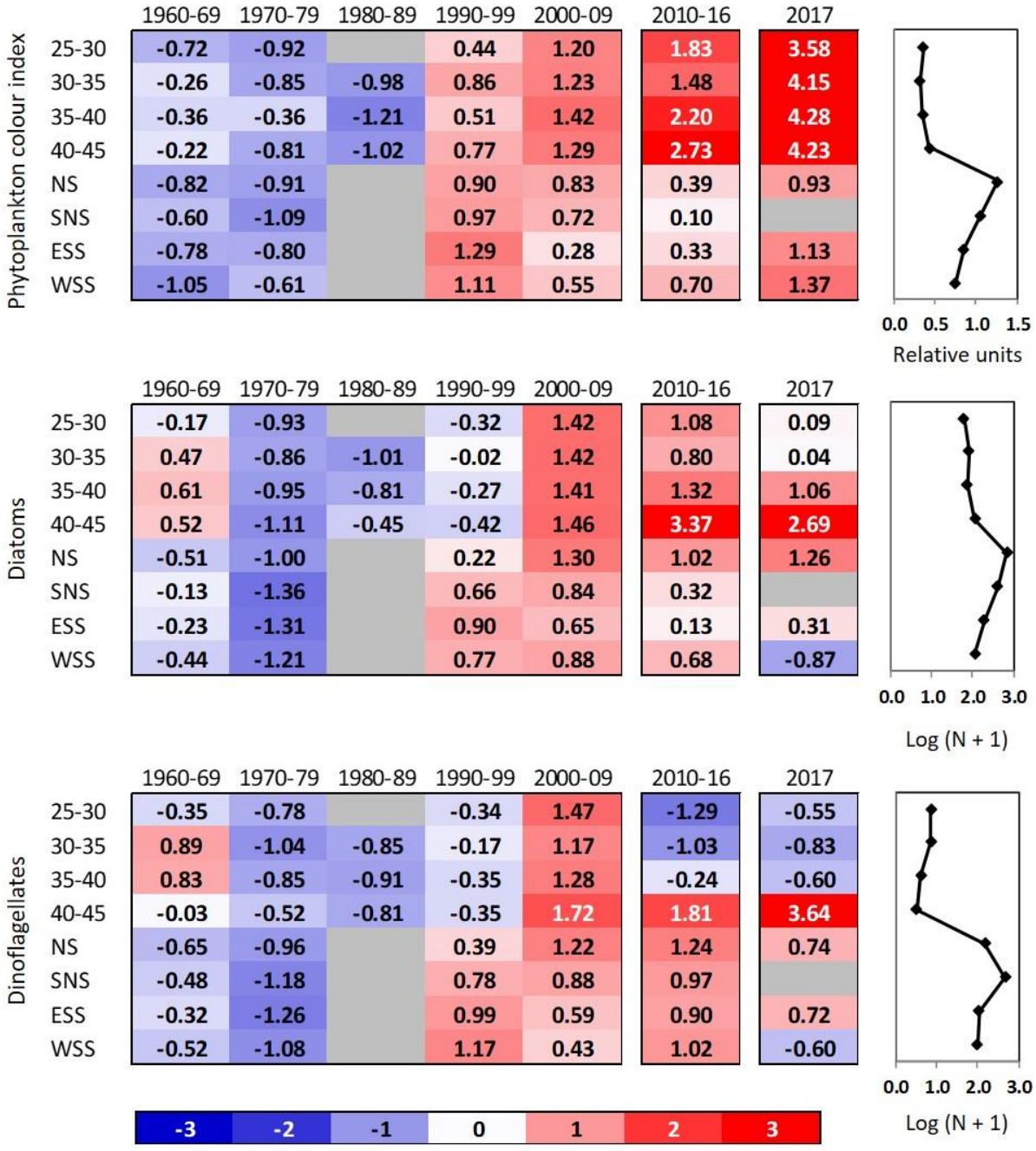

Figure 29. Scorecards for long-term (1960-2017) CPR time series for three indices of phytoplankton concentration in eight regions of the NW Atlantic. Standardised anomalies were calculated using annual averages calculated from monthly averages over decadal (1960-2009), 7 year (2010-2016) or annual (2017) periods, based on climatological averages calculated for the decadal annual averages between 1960 and 2009 (shown in the panels on the right) and standard deviations calculated for the years 1992-2009. Blank cells correspond to years (decades) when sampling was too sparse to give annual (decadal) values. Red (blue) cells indicate higher (lower) than normal values. The numbers in the cells are the standardised anomalies. The regions are: Western Scotian Shelf (WSS), Eastern Scotian Shelf (ESS), South Newfoundland Shelf (SNL), Newfoundland Shelf (NS), and between longitudes 40-45°W, 35-40°W, 30-35°W, 25-30°W.

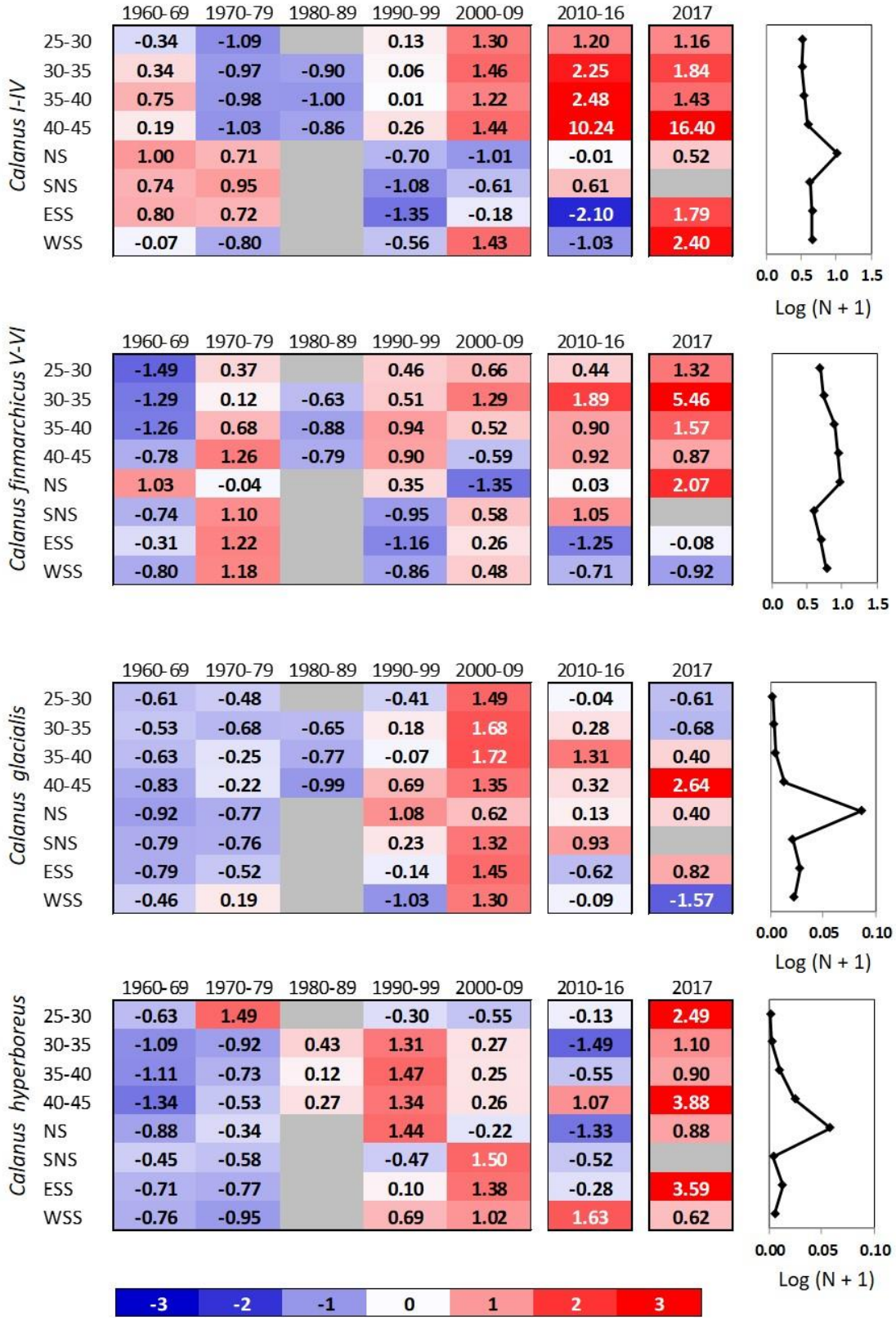

Figure 30. Scorecards for long-term (1960-2016) CPR time series for four Calanus taxa in eight regions in the NW Atlantic. Details as described previously.

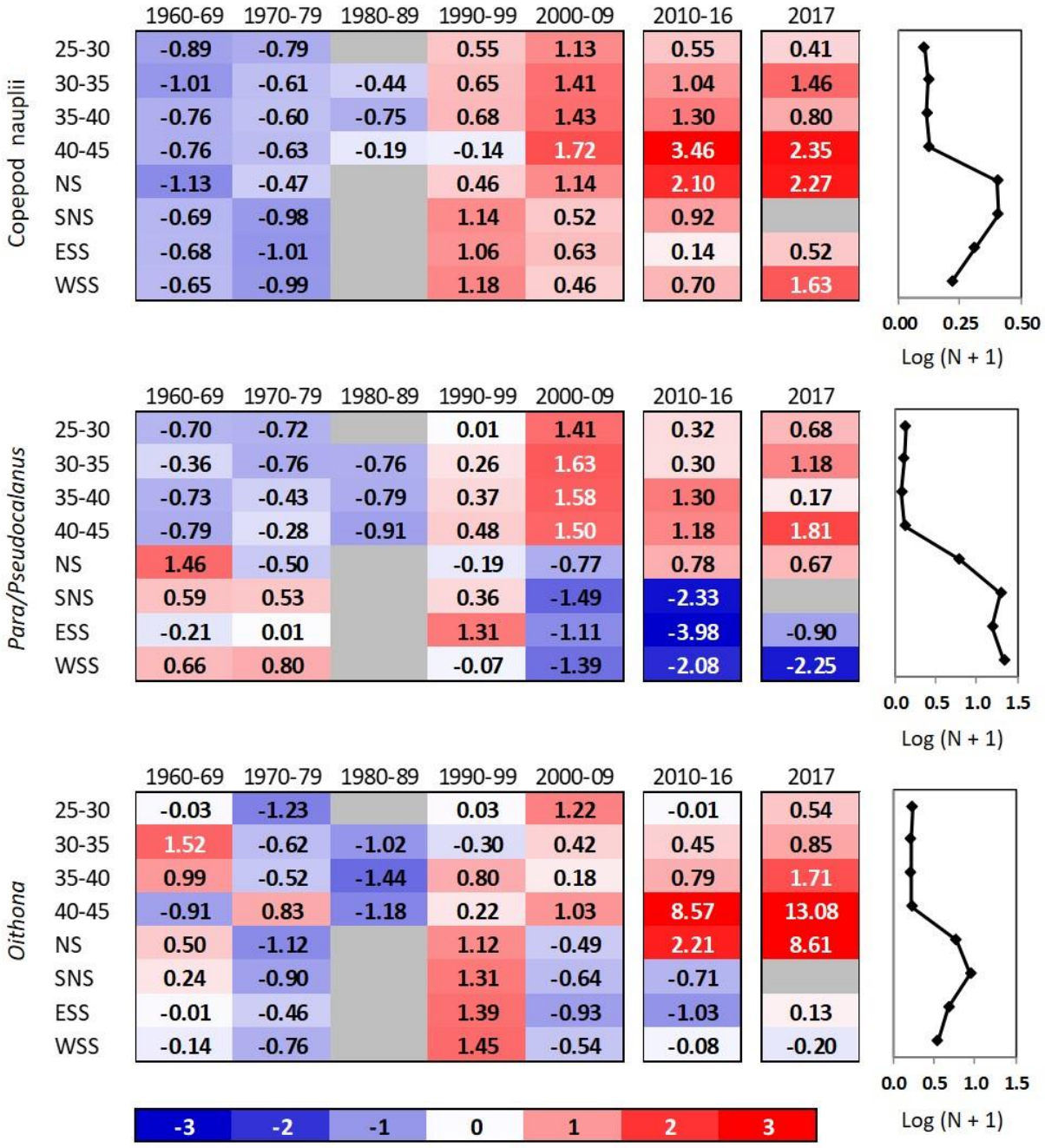

Figure 31. Scorecards for long-term (1960-2017) CPR time series for three small copepod taxa in eight regions in the NW Atlantic. Details as in Figure ??.

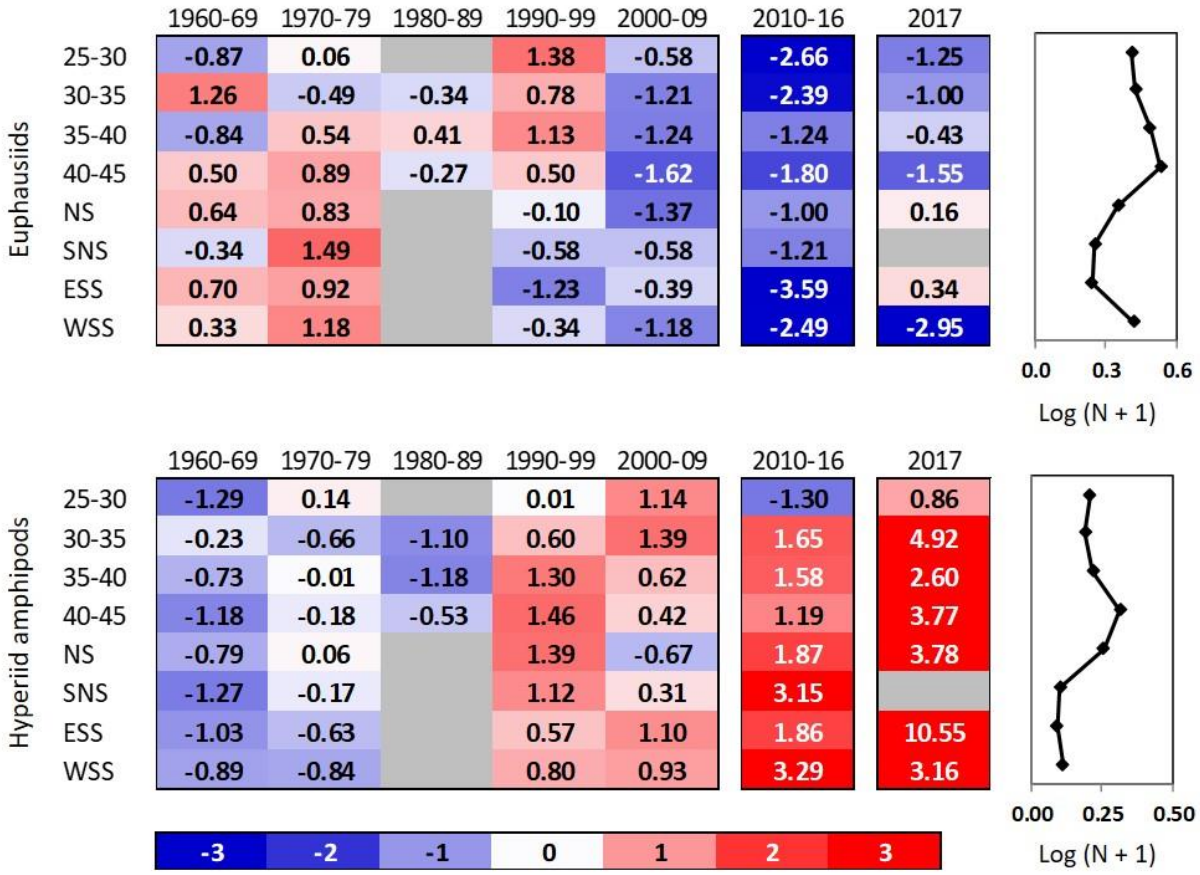

Figure 32. Scorecards for long-term (1960-2017) CPR time series for two macrozooplankton taxa in eight regions in the NW Atlantic. Details as for Figure ??.